

U-series disequilibria in Kick'em Jenny submarine volcano lavas: A new view of time-scales of magmatism in convergent margins

Fang Huang^{a,b,*}, Craig C. Lundstrom^a, Haraldur Sigurdsson^c, Zhaofeng Zhang^a

^a Department of Geology, University of Illinois at Urbana-Champaign, 1301 W. Green Street, Urbana, IL 61801, USA

^b Institute of Geochemistry and Petrology, ETH Zentrum, CH 8092 Zurich, Switzerland

^c Graduate School of Oceanography, University of Rhode Island, Narragansett, RI 02882, USA

Received 2 January 2010; accepted in revised form 10 May 2010; available online 16 October 2010

Abstract

We present data for U and its decay series nuclides ^{230}Th , ^{226}Ra , ^{231}Pa , and ^{210}Po for 14 lavas from Kick'em Jenny (KEJ) submarine volcano to constrain the time-scales and processes of magmatism in the Southern Lesser Antilles, the arc having the globally lowest plate convergence rate. Although these samples are thought to have been erupted in the last century, most have $(^{226}\text{Ra})/(^{210}\text{Po})$ within $\pm 15\%$ of unity. Ten out of 14 samples have significant ^{226}Ra excesses over ^{230}Th , with $(^{226}\text{Ra})/(^{230}\text{Th})$ up to 2.97, while four samples are in ^{226}Ra – ^{230}Th equilibrium within error. All KEJ samples have high $(^{231}\text{Pa})/(^{235}\text{U})$, ranging from 1.56 to 2.64 and high ^{238}U excesses (up to 43%), providing a global end-member of high ^{238}U and high ^{231}Pa excesses. Negative correlations between Sr, sensitive to plagioclase fractionation, and Ho/Sm, sensitive to amphibole fractionation, or K/Rb, sensitive to open system behavior, indicate that differentiation at KEJ lavas was dominated by amphibole fractionation and open-system assimilation. While $(^{231}\text{Pa})/(^{235}\text{U})$ does not correlate with differentiation indices such as Ho/Sm, $(^{230}\text{Th})/(^{238}\text{U})$ shows a slight negative correlation, likely due to assimilation of materials with slightly higher $(^{230}\text{Th})/(^{238}\text{U})$. Samples with ^{226}Ra excess have higher Sr/Th and Ba/Th than those in ^{226}Ra – ^{230}Th equilibrium, forming rough positive correlations of $(^{226}\text{Ra})/(^{230}\text{Th})$ with Sr/Th and Ba/Th similar to those observed in many arc settings. We interpret these correlations to reflect a time-dependent magma differentiation process at shallow crustal levels and not the process of recent fluid addition at the slab–wedge interface.

The high ^{231}Pa excesses require an in-growth melting process operating at low melting rates and small residual porosity; such a model will also produce significant ^{238}U – ^{230}Th and ^{226}Ra – ^{230}Th disequilibrium in erupted lavas, meaning that signatures of recent fluid addition from the slab are unlikely to be preserved in KEJ lavas. We instead propose that most of the ^{238}U – ^{230}Th , ^{226}Ra – ^{230}Th , and ^{235}U – ^{231}Pa disequilibria in erupted KEJ lavas reflect the in-growth melting process in the mantle wedge (reflecting variations in U/Th, daughter–parent ratios, $f\text{O}_2$, and thermal structure), followed by modification by magma differentiation at crustal depths. Such a conclusion reconciles the different temporal implications from different U-series parent–daughter pairs and relaxes the time constraint on mass transfer from slab to eruption occurring in less than a few thousand years imposed by models whereby ^{226}Ra excess is derived from the slab.

© 2010 Elsevier Ltd. All rights reserved.

1. INTRODUCTION

Convergent margins are thought to be the major tectonic setting for forming juvenile continental crust and

recycling of subducted materials back to the convecting mantle. Hydrous fluid is transferred from the subducting slab to the overriding mantle wedge, lowering the solidus of mantle peridotite and inducing partial melting of hydrous mantle peridotite (e.g., Gill, 1981). Indeed, fluxes from slabs (i.e., hydrous fluids and sediment melts) clearly dominate the trace element geochemical properties of convergent margin lavas (e.g., Turner et al., 1996, 1997, 1998, 2000, 2001, 2003; Elliott et al., 1997; Regelous et al.,

* Corresponding author. Current address: Institute of Geochemistry and Petrology, ETH Zentrum, CH 8092 Zurich, Switzerland.

E-mail addresses: huangfang426@hotmail.com, fang.huang@erdw.ethz.ch (F. Huang).

1997; Turner and Hawkesworth, 1997, 1998; Heath et al., 1998; Chabaux et al., 1999; Bourdon et al., 1999; Sigmarsson et al., 2002; George et al., 2003, 2004). An important goal of subduction zone magmatism remains understanding the processes and time scales of melting, slab-mantle transfer and magma ascent and differentiation.

Several intermediate nuclides within the U-series decay chains have half-lives comparable to the time-scales of magmatic processes (e.g., ^{231}Pa ($t_{1/2} = 32.8$ kyr), ^{230}Th ($t_{1/2} = 75.7$ kyr), and ^{226}Ra ($t_{1/2} = 1.6$ kyr)). The differing geochemical behaviors of these elements during dehydration and melting processes result in deviations of the activity ratios of the various parent–daughter pairs from secular equilibrium. Because parent–daughter disequilibrium returns to an activity ratio of unity after five half-lives of the daughter nuclide, U-series data provide a unique tool to constrain the time-scales and thus processes of magmatism in subduction zone settings, including the transfer time-scale of slab components to the overlying mantle wedge. By using three longer lived parent–daughter pairs (^{238}U – ^{230}Th , ^{230}Th – ^{226}Ra , and ^{235}U – ^{231}Pa) in parallel, increased constraints on the interpretations of each system exist, leading to improved identification of the processes forming the disequilibria.

Numerous U-series disequilibrium surveys on young arc lavas have produced two important observations: (1) while the majority of young samples have $(^{238}\text{U})/(^{230}\text{Th})$ greater than unity, a significant number do have $(^{238}\text{U})/(^{230}\text{Th}) < 1$; and (2) most young samples have $(^{226}\text{Ra})/(^{230}\text{Th})$ and $(^{231}\text{Pa})/(^{235}\text{U}) > 1$ (e.g., Gill and Williams, 1990; Turner et al., 1996, 1997, 1998, 2000, 2001, 2003, 2006; Pickett and Murrell, 1997; Turner and Hawkesworth, 1997, 1998; Heath et al., 1998; Bourdon et al., 1999; Chabaux et al., 1999; Turner and Foden, 2001; Sigmarsson et al., 2002; Thomas et al., 2002; Dosseto et al., 2003; Peate and Hawkesworth, 2005; Asmerom et al., 2005; Dufek and Cooper, 2005; DuFrane et al., 2006; Garrison et al., 2006; Reagan et al., 2006; Huang and Lundstrom, 2007; Toothill et al., 2007; Touboul et al., 2007). However, although these features are observed universally in arcs, there remains substantial debate about which processes and mechanism generate these disequilibria. Namely, the main issue is whether the disequilibria that are observed in erupted lavas reflect processes of fluid transfer at the slab–wedge interface or whether such signatures are erased by subsequent processes occurring within the mantle wedge during partial melting. Answering this question is important as it dictates whether the observed ^{226}Ra excesses place constraints on the time from slab to the Earth's surface or only from some location in the shallow mantle or even crust where reaction between melt and coexisting minerals ceases.

Relatively few studies have focused on examining the U-series disequilibrium variations in a suite of samples from a single volcano. However, because shallow crustal-level magma differentiation processes can significantly modify U-series disequilibria in young lavas (Vigier et al., 1999; Blake and Rogers, 2005; Garrison et al., 2006; Touboul et al., 2007; Price et al., 2007; Huang et al., 2008), studies of single volcanic systems are needed to identify such processes. Because determination of magma ascent rates depends on discriminating a disequilibrium signature pro-

duced prior to shallow crustal differentiation, it is critically important to evaluate the effect of shallow differentiation processes on U-series disequilibria.

In this study, we present U–Th–Ra–Po and U–Pa data from a suite of samples ranging in composition from basalt to basaltic andesite from Kick'em Jenny (KEJ hereafter) submarine volcano in the Southern Lesser Antilles arc. This paper is a straightforward extension of our earlier work documenting the large ^{235}U – ^{231}Pa disequilibria in KEJ lavas (Huang and Lundstrom, 2007); in that work, we focused on the tectonic control of convergence rate in producing ^{235}U – ^{231}Pa disequilibrium globally in subduction zone settings. Here our goals are to determine the effect of magma differentiation on ^{238}U – ^{230}Th – ^{226}Ra disequilibria in a single volcano and to interpret the remaining U-series disequilibrium behavior in terms of mantle melting processes in order to sort out whether signatures of slab fluid transfer are preserved in erupted lavas. The data are then used to constrain the timing and processes of magmatism in the Southern Lesser Antilles and offer a guide to future modeling of global subduction zone volcanic processes.

2. GEOLOGICAL BACKGROUND AND SAMPLE DESCRIPTIONS

The geological background of the Lesser Antilles arc has been discussed extensively in the literature (Hawkesworth et al., 1979; Speed et al., 1993; Devine and Sigurdsson, 1995; Devine, 1995; Turner et al., 1996; Heath et al., 1998; Macdonald et al., 2000; Zellmer et al., 2003; Toothill et al., 2007; DuFrane et al., 2009). Briefly, the Lesser Antilles arc is ~800 km long, formed by westward subduction of the Atlantic oceanic plate beneath the Caribbean plate (Fig. 1). The arc can be divided into two segments, a northern zone defined by portions north of Martinique and a southern zone south thereof. The change in obliquity of subduction along the arc results in significantly lower convergence rate in the south (~1.3 cm/yr) than the north (3.7 cm/yr) (Jarrard, 1986; Speed et al., 1993). A double arc occurs north of Dominica, while it is not obvious in the Southern Lesser Antilles arc (Macdonald et al., 2000). The northern zone has a slab dip of 50–60° while the southern zone ranges from a slab dip of 45–50° in the north to almost vertical in the south (Wadge and Shepherd, 1984). Magma production rates in the Lesser Antilles are low (4 km³/Ma per km of arc) over the past 100,000 years, which may be due to the slow convergence rate (Wadge and Shepherd, 1984). Magma production is greatest in the central arc, possibly reflecting the change in slab dip and obliquity of subduction (Macdonald et al., 2000). The Lesser Antilles arc has the thickest crust (~35 km) of all island arcs (Gill, 1981; Plank and Langmuir, 1998).

Geochemical studies have shown that primary magmas erupted in the Lesser Antilles arc result from melting of depleted mid-ocean ridge basalt (MORB)-type mantle that has been metasomatized by fluid and sediment components derived from the subducted Atlantic oceanic slab (Turner et al., 1996; Macdonald et al., 2000). Magma compositions systematically vary along the arc from low-K tholeiites in the north, to higher-K calc-alkaline lavas in the central

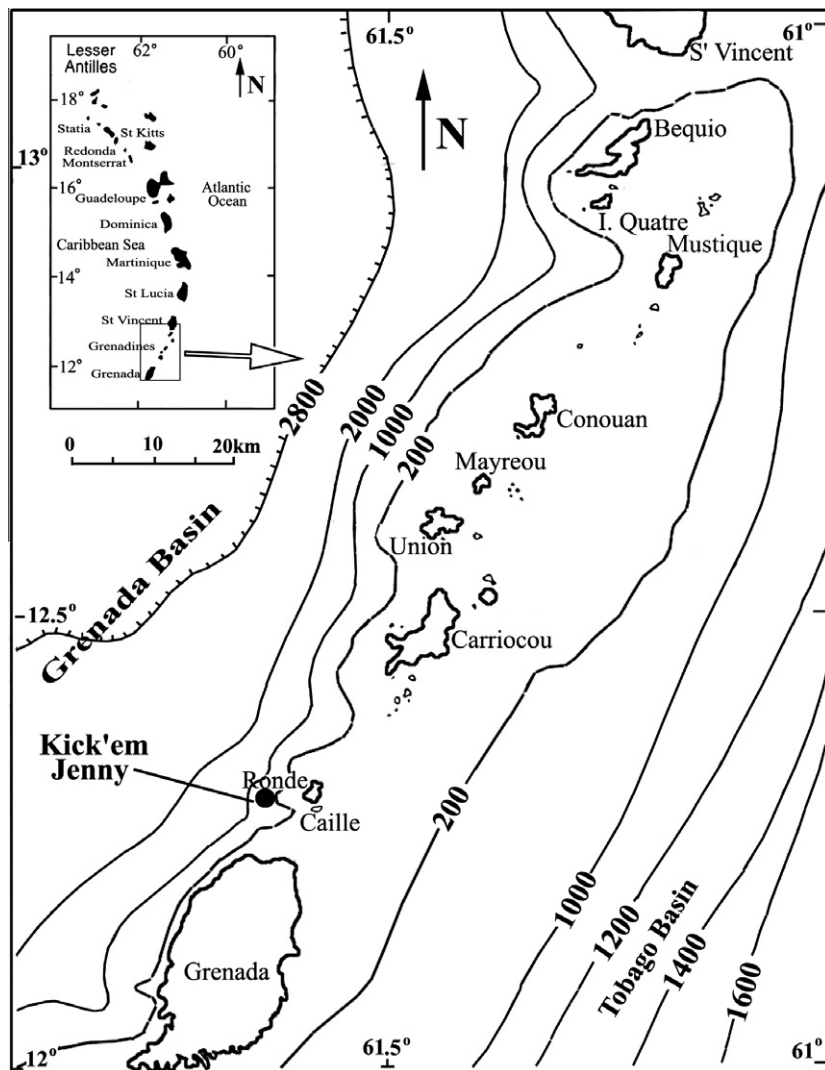


Fig. 1. Geologic background of Kick'em Jenny submarine volcano and the Lesser Antilles arc. Revised from Devine and Sigurdsson (1995) and Turner et al. (1996).

region and alkaline lavas in the south. The along-arc variation of major element compositions is mirrored in trace element and radiogenic isotopic compositions. For instance, lavas from the Southern Lesser Antilles have lower Ba/Th and more radiogenic Pb and Sr isotope ratios than those of the Northern Lesser Antilles; this is interpreted to reflect a southward increase in the relative contribution of sediment components compared to fluid components (Turner et al., 1996). The Southern Lesser Antilles arc contains lavas with the highest average $(^{231}\text{Pa})/(^{235}\text{U})$ from any convergent margin, likely attributable to this location having the lowest convergence rate of any subduction zone (Turner et al., 2006; Huang and Lundstrom, 2007).

KEJ volcano is located ~ 9 km to the north of Grenada in the Southern Lesser Antilles (Devine and Sigurdsson, 1995) (Fig. 1). The summit depth of KEJ volcano was surveyed in 1978 as 160 m below sea level. Several eruptions in the last century make KEJ an excellent location to study submarine eruptions of an island arc volcano (Devine and Sigurdsson, 1995). Our samples were collected by dredging

from the crater environment of Kick'em-Jenny submarine volcano ($12^{\circ}30'\text{N}$, $61^{\circ}38'\text{W}$) in 1972 (Sigurdsson and Shepherd, 1974; Devine and Sigurdsson, 1995); these samples were most likely derived from 20th century eruptions, principally the 1939 eruption. Therefore, the ageing effect after eruption on ^{238}U - ^{230}Th - ^{226}Ra and ^{235}U - ^{231}Pa data should be negligible. Fourteen whole rock samples with compositions ranging from basalt to basaltic andesite were selected for U-series disequilibrium analysis. Note that $(^{231}\text{Pa})/(^{235}\text{U})$ and U-Th contents for all but two of these samples (porphyritic olivine basalts KEJ010 and KEJ017) were reported in Huang and Lundstrom (2007). Further details of the mineralogy and petrology of the KEJ lavas can be found in Devine and Sigurdsson (1995).

3. ANALYTICAL METHODS

After the samples were crushed into ~ 5 mm sized chips, fresh pieces without visible alteration or secondary veins were handpicked and cleaned in an ultrasonic bath for

10 min with ultra-pure water 3 times to remove any adhered seawater. Rock chips were then powdered in methanol using an agate mortar.

Trace element compositions of KEJ010, KEJ017, KEJ100, KEJ101, KEJ103, and KEJ1976 were measured at the GeoAnalytical Lab of Washington State University using a Sciex Elan model 250 Inductively Coupled Plasma Mass Spectrometry (ICP-MS) (Table 1) (Knaack et al., 1994; Knaack, 2003). Long term precision is better than 5% (RSD) for the rare earth elements and 10% for the other trace elements based on analyses of USGS and international rock standards. Sr isotope ratios were measured by a Nu-Plasma HR multi-collector ICP-MS (MC-ICP-MS) in the Dept. of Geology at the University of Illinois at Urbana-Champaign (UIUC). Sr was purified using Sr-Spec resin with a procedural blank <1 ng. Instrumental mass fractionation was corrected using an exponential law and $^{86}\text{Sr}/^{88}\text{Sr} = 0.1194$. Measurement of BCR-2 gave $^{87}\text{Sr}/^{86}\text{Sr} = 0.705005 \pm 40$ (2σ , $n = 3$).

U, Th, Pa, and Ra concentrations were determined using the Nu-Plasma MC-ICP-MS at UIUC by isotope-dilution methods involving enriched isotopic spikes of ^{228}Ra , ^{229}Th , ^{233}Pa , and ^{236}U . Separations for U and Th were based on chromatographic methods using anion exchange resin. Ra was separated using cation exchange resin (AG50-X8) followed by two Sr-spec resin columns to remove Ba. The Pa separation followed procedures given in Regelous et al. (2004). Typical procedural blanks are <0.1 fg for ^{226}Ra and ^{231}Pa , and <10 pg for Th and U. ^{210}Po was analyzed by isotope dilution alpha spectrometric methods using ^{209}Po as a spike. Chemistry and plating of ^{210}Po were done at UIUC with alpha spectrometry performed at the University of Iowa. Chemical separation for Po follows procedures given in Reagan et al. (2005, 2006).

The accuracy of ^{238}U – ^{230}Th and ^{230}Th – ^{226}Ra activity ratio determinations was checked by measurements of rock standards ATHO and BCR-2; the accuracy of ^{235}U – ^{231}Pa

Table 1
Major (wt.%) and trace element (ppm) compositions of six Kick'em Jenny samples.

	KEJ010	KEJ017	KEJ100	KEJ101	KEJ103	KEJ1976
SiO ₂	52.58	47.58	51.74	48.56	53.85	
TiO ₂	0.87	1	0.86	1.13	0.75	
Al ₂ O ₃	19.44	16.59	19.37	18.49	19.48	
Fe ₂ O ₃	8.40	9.29	8.71	9.30	8.08	
MnO	0.18	0.15	0.13	0.11	0.16	
MgO	4.87	11.85	5.38	7.79	4.39	
CaO	9.71	11.13	9.72	12.11	9.19	
Na ₂ O	3.17	2.07	3.17	2.40	3.51	
K ₂ O	1.11	0.51	0.93	0.68	1.13	
P ₂ O ₅	0.24	0.26	–	–	–	
Total	100.33	100.17	100.01	100.57	100.54	
Sc	28.8	55.1	37.6	58.8	18.2	52.5
Rb	46.0	14.2	33.3	20.2	25.7	22.8
Sr	343	266	333	287	485	300
Y	22.6	18.5	21.2	21.0	23.1	21.8
Zr	96	49	86	64	112	70
Nb	4.94	2.77	5.09	3.86	10.08	4.18
Cs	1.80	0.65	1.26	0.65	1.01	0.71
Ba	206	95	186	135	273	151
La	9.21	4.11	8.80	6.10	19.38	6.75
Ce	18.9	9.5	18.3	13.5	36.5	14.5
Pr	2.43	1.40	2.43	1.90	4.35	2.02
Nd	10.4	7.0	10.6	8.9	17.1	9.2
Sm	2.84	2.25	2.88	2.70	3.76	2.77
Eu	0.98	0.85	1.05	1.01	1.25	1.02
Gd	3.31	2.90	3.44	3.34	3.95	3.54
Tb	0.61	0.53	0.60	0.62	0.66	0.63
Dy	4.13	3.55	3.98	4.15	4.30	4.21
Ho	0.89	0.76	0.85	0.85	0.93	0.89
Er	2.59	2.02	2.37	2.34	2.61	2.45
Tm	0.38	0.29	0.35	0.34	0.40	0.36
Yb	2.51	1.83	2.26	2.17	2.63	2.28
Lu	0.41	0.29	0.36	0.33	0.42	0.35
Hf	2.71	1.58	2.49	2.01	2.98	2.17
Ta	0.34	0.19	0.34	0.25	0.65	0.28
Eu* ^a	1.05	0.98	1.03	0.97	0.99	1.00

^a Eu* = $\text{Eu}_N / (\text{Sm}_N \times \text{Gd}_N)^{1/2}$, N is the value normalized by C1-chondrite (McDonough and Sun, 1995). Major elements data are from Devine and Sigurdsson (1995).

Table 2

U-series data, Sr isotopes, Mg#, Ba/Th, Sr/Th, Ho/Sm, and K/Rb of KEJ submarine volcano.

Samples	U (ppm)	^{(234U)/} ^(238U)	Th (ppm)	U/ Th	^{(230Th)/} ^(238U)	^{(230Th)/} ^(232Th)	^{(238U)/} ^(232Th)	^{226Ra} (fg/g)	^{(226Ra)/} ^(230Th)	Pa (fg/g)	^{(231Pa)/} ^(235U)	^{210Po} (dpm/g)	^{(226Ra)/} ^(210Po)	^{87Sr/} ^{86Sr}	Mg#	Ba/ Th	Sr/ Th	Ho/ Sm	K/ Rb
RB07	0.982	0.995	2.515	0.390	0.875	1.036	1.184	862	2.970	833	2.61	1.95	0.97	0.705900	45.6	73.0	123.7	0.249	353
Duplicate										834	2.61								
Duplicate										863	2.70								
Average										843	2.64								
RB47	4.876	0.993	10.780	0.452	0.793	1.088	1.372	1247	0.954	2975	1.88	2.47	1.11	0.705326	54.4	38.1	40.9	0.179	115
Duplicate								1266	0.968	2975	1.88								
Duplicate								1273	0.974										
Average								1262	0.965	2975	1.88								
RB51b	1.813	0.989	3.863	0.469	0.728	1.037	1.424	787	1.763	1343	2.28			0.706326	54.0	60.6	102.3	0.299	196
RB64	2.184	0.998	5.120	0.427	0.778	1.008	1.296	605	1.053	1679	2.36	1.20	1.11	0.705592	64.2	44.6	75.5	0.230	170
Duplicate								589	1.025										
Average								597	1.039										
RB65	2.007	0.987	5.302	0.379	0.866	0.994	1.148	568	0.967	1724	2.64	1.41	0.89	0.705573	62.0	44.9	80.1	0.223	176
Duplicate								560	0.954										
Average								564	0.961										
RB79	0.535	0.996	1.252	0.427	0.815	1.058	1.298	308	2.089	271	1.56			0.705384	61.2	85.3	225.2	0.321	232
RB82	0.929	0.998	1.830	0.508	0.707	1.089	1.540	493	2.220	704	2.33			0.705675	65.2	74.6	174.0	0.311	263
KEJ010	1.875	0.996	3.810	0.492	0.716	1.068	1.492	805	1.813	1395	2.29			0.706373	53.7	53.9	89.6	0.314	89
Duplicate	1.904	0.992	3.858	0.494	0.690	1.032	1.496	813	1.830	1376	2.22								
Duplicate	1.908	0.996	3.861	0.494	0.689	1.032	1.498	1405	2.26										
Average	1.896	0.995	3.843	0.493	0.698	1.044	1.495	809	1.822	1392	2.26								
KEJ017	0.577	1.000	1.146	0.503	0.726	1.108	1.526	315	2.227	417	2.23			0.705636	71.8	83.4	232.2	0.336	299
Duplicate	0.575	1.001	1.138	0.505	0.725	1.110	1.532	317	2.253	422	2.26								
Duplicate	0.589	0.999	1.168	0.504	0.726	1.110	1.529	308	2.130										
Average	0.580	1.000	1.151	0.504	0.726	1.109	1.529	313	2.20	420	2.25								
KEJ100	1.574	0.998	3.141	0.501	0.708	1.076	1.520	1036	2.749	1123	2.21	1.98	1.14	0.705806	55.3	61.3	109.8	0.294	232
Duplicate	1.572		3.161	0.497	0.712	1.075	1.510	1032	2.727										
Duplicate	1.539		3.126	0.492	0.719	1.074	1.494	1033	2.762										
Average	1.562		3.143	0.497	0.713	1.075	1.508	1034	2.746										
KEJ100* ^a	1.840	1.00	3.090	0.595	0.63		1.14			1292	2.15								
KEJ101	1.013	1.005	2.000	0.507	0.699	1.074	1.536	530	2.212	755	2.29	1.26	0.92	0.705762	62.6	65.3	138.9	0.317	279
KEJ103	3.149	0.998	6.743	0.467	0.897	1.271	1.417	1031	1.080	2106	2.06	3.59	0.63	0.705605	52.1	37.6	67.0	0.246	365
Duplicate								954	0.999										
Average								993	1.040										
KEJ899	1.689	0.989	3.365	0.502	0.703	1.071	1.523	790	1.969	1266	2.30			0.705801	51.9	63.4	114.1	0.273	200
KEJ1976	1.173	0.992	2.360	0.497	0.705	1.062	1.506	593	2.124	878	2.29			0.705844	64.6	128.7	0.320		
ATHO	2.234	0.995	7.471	0.299	1.138	0.907	0.906	854	0.999										
2stddev	0.024	0.006	0.033	0.003	0.031	0.07	0.09	29	0.033										
BCR-2	1.696	0.997	5.907	0.287	1.002	0.872	0.870			551	1.00								
2stddev	0.003	0.002	0.001	0.000	0.003	0.008	0.000			28	0.05								
RGM-1												4.18							

^a U-Th data of KEJ100* are from Gill and Williams (1990) and Pa data are from Williams and Perrin (1989). Pa, U, and Th contents are from Huang and Lundstrom (2007) except KEJ010 and KEJ017. U-Th-Pa-Ra data were analyzed by isotope-dilution methods using MC-ICP-MS. ATHO was measured 5 times for U and Th and 3 times for Ra. BCR-2 was measured 3 times for U and Th and 6 times for Pa. Po content was measured by alpha counting.

determination was verified using BCR-2 (Table 2). Duplicated analyses of ATHO show typical external precision for U concentrations of ~1%, Th ~0.4%, and ^{226}Ra ~3%, while the ^{231}Pa reproducibility is estimated as 5% based on measurements of BCR-2 (2 σ). The U, Th and ^{231}Pa concentrations and ($^{230}\text{Th}/^{232}\text{Th}$) of these two standards are in good agreement with recommended values in the literature (Prytulak et al., 2008; Sims et al., 2008; Koornneef et al., 2010). Duplicate U-series analyses for samples also show good agreement (Table 2). Accuracy of ^{210}Po analysis was checked by measuring USGS rhyolite standard RGM-1; the activity for ^{210}Po in RGM-1 is 4.18 ± 0.06 (dpm/g, 2 σ), consistent with the result (4.23 ± 0.07 dpm/g) given in Reagan et al. (2005). The error of a single sample analysis was estimated to be 9% to 15% (2 σ) based on the number of ^{210}Po counts (200–500) collected by alpha counter.

4. RESULTS

4.1. Major and trace elements

Compositionally, the KEJ samples range from 47.2 to 55.5 wt.% SiO_2 with Mg# between 30 and 73 (Devine and Sigurdsson, 1995; Huang and Lundstrom, 2007; Table 2). The corresponding major and trace element compositions of six samples not previously published are reported in Table 1. The Sr, Ba, Rb, Zr, and Y contents of KEJ010, KEJ017, KEJ 100, KEJ101, and KEJ103 were previously reported in Devine and Sigurdsson (1995); the new data presented here generally agree with these previous data.

In detail, the KEJ samples are enriched in large ion lithophile elements (LILE, e.g., U and K) and depleted in high field strength elements (HFSE, e.g., Ta and Nb), as is typical for arc magmas (Fig. 2A). Notably, in contrast with other arcs such as the Northern Lesser Antilles, Tonga, and Kermadec (e.g., Turner et al., 1996, 1997), Ba concentrations are depleted relative to Cs, Th, and U. Ra and Pa are also normalized to their values in a primitive mantle in U-series secular equilibrium in Fig. 2; this shows that Pa and Ra are enriched relative to many highly fluid-mobile elements such as Ba and Rb. KEJ lavas have low Sr/Th (41–232) and Ba/Th (37.6–85.3), compared with other arc lavas globally (Fig. 3A and B), suggesting a larger contribution of sediment to the mantle source. Sr/Th of KEJ lavas is generally negatively correlated with SiO_2 , consistent with magma differentiation, while the variable Sr/Th in the low SiO_2 (<50 wt.%) samples more likely reflects source heterogeneity (Fig. 3A).

REE patterns vary from slightly light rare earth element (LREE) enriched to strongly LREE enriched patterns (Fig. 2B). La and Lu contents vary significantly with a range of 9.5–36.5 ppm and 1.6–3.0 ppm, respectively, while middle REE generally show smaller ranges than LREE and heavy REE. Eu does not show a significant anomaly relative to Sm and Gd with Eu* ranging from 0.97 to 1.05 (Table 1). Similar to an important observation from Davidson et al. (2007), KEJ lavas show a negative correlation between SiO_2 and Dy/Yb (Table 1), documenting the role of amphibole fractionation in magma differentiation.

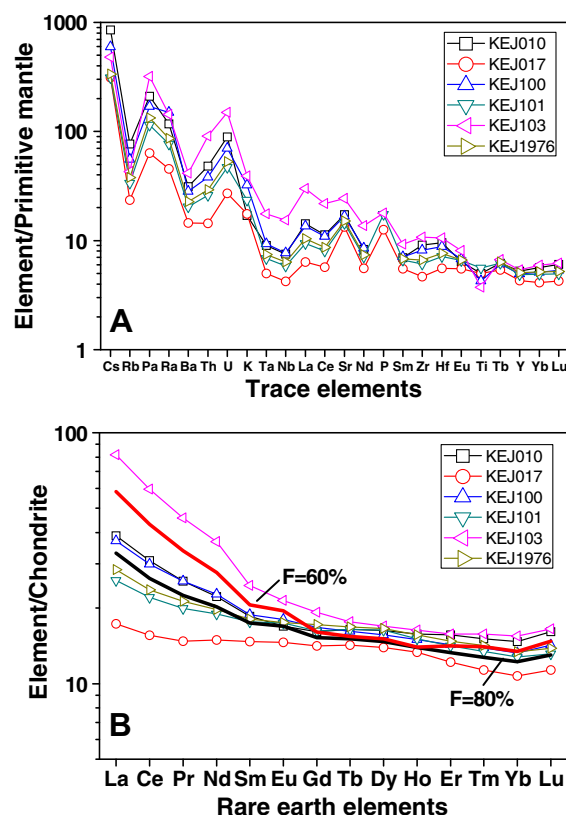


Fig. 2. (A) Primitive mantle normalized trace element patterns. (B) Chondrite-normalized REE patterns. The solid bold lines are the results of the AFC model (DePaolo, 1981). Assuming KEJ017 as the most primitive magma, the AFC model can generally simulate the REE patterns of the KEJ samples with F (fraction of magma remaining in magma chamber) varying up to 60%. The parameters used in the AFC model are given in Table 3. Chondrite and primitive mantle data are from McDonough and Sun (1995); Pa and Ra data are calculated assuming that the primitive mantle is in U-series secular equilibrium. U and Th contents are from Table 2, and other trace element data are from Table 1.

However, because Ho/Sm best captures the amphibole fractionation signature (the amphibole partition coefficients peak at D_{Ho}) and also negatively correlates with SiO_2 , we use Ho/Sm as the best indicator of magma differentiation in KEJ lavas.

4.2. Sr isotopes

All KEJ samples have moderately enriched Sr isotope ratios with $^{87}\text{Sr}/^{86}\text{Sr}$ ranging from 0.7056 to 0.7064, consistent with previously reported values for KEJ (Turner et al., 1996) and M-series basalts from Grenada (Thirlwall et al., 1996), but significantly higher than Northern Lesser Antilles lavas and Grenadan C-series basalts (Thirlwall et al., 1996; Turner et al., 1996). This follows the inference based on trace elements that a greater contribution of a sediment component exists in KEJ lavas (Macdonald et al., 2000). Furthermore, there is no correlation between $^{87}\text{Sr}/^{86}\text{Sr}$ and magma differentiation indices such as SiO_2 and Mg#, suggesting that assimilation of sediments during magma differentiation may be insignificant.

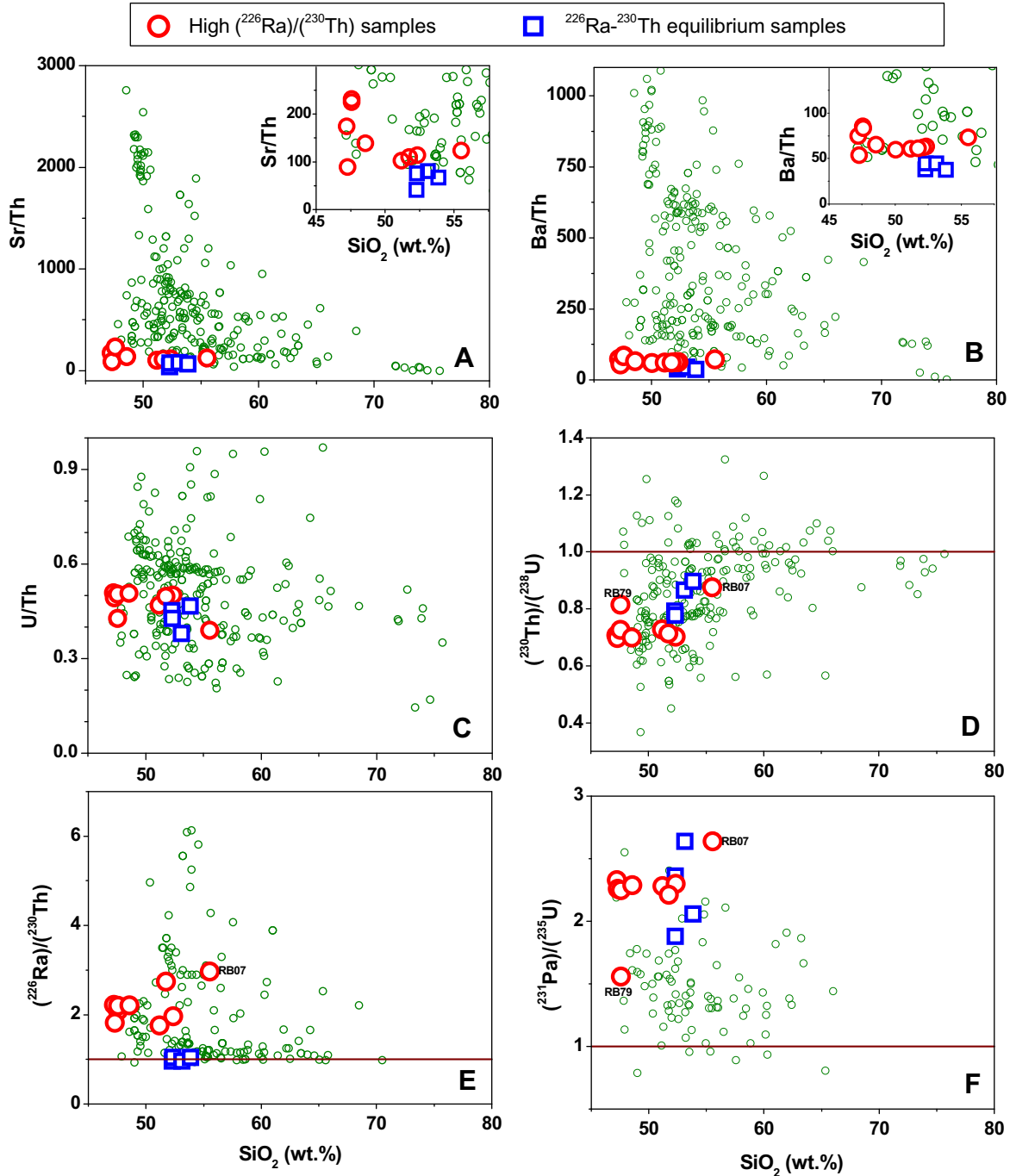


Fig. 3. Correlations of SiO_2 with Sr/Th , Ba/Th , U/Th , and U-series disequilibria of KEJ lavas. Global arc lavas (small open circle) with U-series disequilibrium data are also plotted for a comparison. Inserts in (A) and (B) show that Sr/Th and Ba/Th of KEJ lavas generally decrease with increasing SiO_2 . Data source: Pickett and Murrell (1997), Elliott et al. (1997), Bourdon et al. (1999), Chabaux et al. (1999), Turner and Foden (2001), Thomas et al. (2002), Sigmarsson et al. (2002), Yokoyama et al. (2003), Zellmer et al. (2003), Dosseto et al. (2003), George et al. (2003), Turner et al. (1996, 1997, 2000, 2003, 2006), Asmerom et al. (2005), Garrison et al. (2006), Touboul et al. (2007), and Huang and Lundstrom (2007).

4.3. U-series disequilibria

The results of U-series isotope analyses are listed in Table 2. $(^{234}\text{U})/(^{238}\text{U})$ of the KEJ samples are all within error of unity, given the 2σ uncertainty of ~ 0.006 (based on five analyses of ATHO), indicating that seawater con-

tamination/alteration is insignificant. Based on the premise that these KEJ samples were most likely erupted in the past 100 years, post-eruption decay of $(^{238}\text{U})/(^{230}\text{Th})$, $(^{231}\text{Pa})/(^{235}\text{U})$, and $(^{226}\text{Ra})/(^{230}\text{Th})$ should be negligible. All samples except KEJ103 have $(^{226}\text{Ra})/(^{210}\text{Po})$ within errors of unity. This could be taken to mean that ages might be

greater than 120 years; however it is also consistent with the observation that most young arc lavas erupt with $(^{226}\text{Ra})/(^{210}\text{Po}) = 1$ (Turner et al., 2004; Berlo and Turner, 2010). The exception, KEJ103, has $(^{226}\text{Ra}/^{210}\text{Po})$ of 0.63 and $(^{226}\text{Ra})/(^{230}\text{Th})$ of 1.04.

The $(^{226}\text{Ra})/(^{230}\text{Th})$ of these samples show wide variation with 10 out of 14 KEJ samples having $(^{226}\text{Ra})/(^{230}\text{Th})$ from 1.76 to 2.97, indicating general youthfulness (erupted within the last 8000 yrs); the other four samples (Rb47, Rb64, Rb65, and KEJ103) have $(^{226}\text{Ra})/(^{230}\text{Th})$ within 4% of unity, which we conservatively take to indicate secular equilibrium. The KEJ lavas can be divided into two groups based on their $(^{226}\text{Ra})/(^{230}\text{Th})$ behavior and this grouping holds for several other geochemical properties as well. Except for RB07, high ^{226}Ra excess samples are characterized by having higher Ho/Sm, K/Rb, Sr/Th, Ba/Th, and SiO_2 , but lower Sr contents and La/Yb (not shown) relative to the four samples close to ^{226}Ra – ^{230}Th equilibrium (Figs. 3 and 4). Combined with previous data (Turner et al., 1996; Heath et al., 1998; Zellmer et al., 2003), our re-

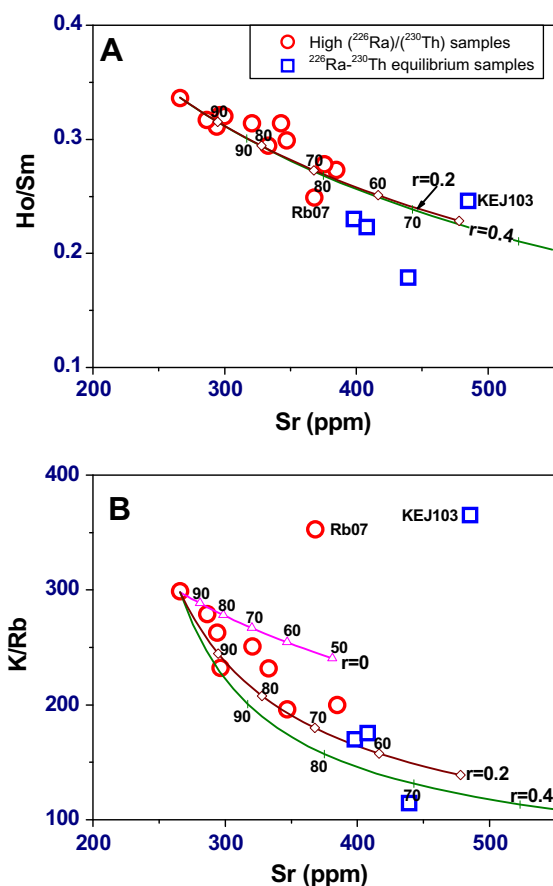


Fig. 4. Sr contents against (A) Ho/Sm and (B) K/Rb for the KEJ samples grouped by the $(^{226}\text{Ra})/(^{230}\text{Th})$ values in this study. The negative correlations between Sr and Ho/Sm and K/Rb cannot be explained by only fractional crystallization ($r = 0$), where r is the assimilation/crystallization ratio. Assimilation is required to decrease K/Rb. The parameters used in the AFC model are from Table 3. Fraction of magma remaining (F) is marked in percentage (%). Sr, Ho/Sm, and K/Rb data are from Table 1 and 2, Devine and Sigurdsson (1995).

sults show that the positive correlation between $(^{238}\text{U})/(^{230}\text{Th})$ and $(^{226}\text{Ra})/(^{230}\text{Th})$ observed in Chabaux et al. (1999) is statistically valid (Fig. 5B).

U and Th contents of KEJ lavas measured by ICP-MS are consistent with the isotope-dilution determinations and generally increase with SiO_2 content. U varies from 0.54 to 4.88 ppm and Th from 1.15 to 10.78 ppm, while U/Th shows less variability ranging from 0.38 to 0.51 (Table 2). All KEJ samples show significant ^{238}U excess over ^{230}Th , consistent with previous results for KEJ lavas (Gill and Williams, 1990; Turner et al., 1996). The $(^{230}\text{Th})/(^{238}\text{U})$ (0.698–0.728 excepting Rb07 of 0.875) of samples with high ^{226}Ra excess are generally lower than that of the four samples close to ^{226}Ra – ^{230}Th equilibrium (0.778–0.897) (Table 2 and Fig. 5). Combining all KEJ samples except KEJ103 with samples from adjacent Ile de Caille island (Turner et al., 1996) forms a linear correlation across the $(^{230}\text{Th})/(^{232}\text{Th})$ – $(^{232}\text{Th})/(^{238}\text{U})$ equiline diagram (Fig. 5A). It is unclear why KEJ103 has higher $(^{230}\text{Th})/(^{232}\text{Th})$ (1.27) and $(^{230}\text{Th})/(^{238}\text{U})$ (0.897) than other KEJ samples.

The KEJ samples have very high ^{231}Pa excesses with $(^{231}\text{Pa})/(^{235}\text{U})$ ranging from 1.56 to 2.64; there is no obvious difference between ^{231}Pa excess in the samples with high ^{226}Ra excesses and those near ^{226}Ra – ^{230}Th equilibrium (Fig. 5C). KEJ010 and KEJ017 have similar $(^{231}\text{Pa})/(^{235}\text{U})$ of 2.26 and 2.25, respectively, consistent with the high $(^{231}\text{Pa})/(^{235}\text{U})$ ratios previously observed in the samples from KEJ and other volcanoes from the Southern Lesser Antilles arc (Pickett and Murrell, 1997; Turner et al., 2006; Huang and Lundstrom, 2007). Notably, although RB07 is the most differentiated sample based on high SiO_2 and low Mg#, it has the highest ^{231}Pa excess (2.64) and ^{226}Ra excess (2.97). $(^{231}\text{Pa})/(^{235}\text{U})$ is not correlated with magma differentiation indices such as Ho/Sm (Fig. 6B), K/Rb, La/Yb, Mg#, and SiO_2 content, indicating that magma differentiation does not significantly modify $(^{231}\text{Pa})/(^{235}\text{U})$ of the KEJ samples. The correlation between $(^{231}\text{Pa})/(^{235}\text{U})$ and $(^{230}\text{Th})/(^{238}\text{U})$ does not follow the trend of addition of U-enriched hydrous fluid (Fig. 5D). Finally, KEJ samples have both high $(^{231}\text{Pa})/(^{235}\text{U})$ and $(^{238}\text{U})/(^{230}\text{Th})$, and the highest average $(^{231}\text{Pa})/(^{230}\text{Th})$ of all arc lavas providing a conundrum to simple models of U-rich fluid addition.

5. DISCUSSION

Because time-dependent magma differentiation processes can significantly modify the U-series disequilibria in young lavas (e.g., Price et al., 2007; Touboul et al., 2007; Huang et al., 2008), we first focus on assessing how the magma differentiation process affects U-series disequilibria in KEJ lavas. We then apply our KEJ data to the problem of constraining the time-scales and processes of magma generation and ascent in a subduction zone having a low convergence rate.

5.1. Magma differentiation in KEJ submarine volcano

Few if any convergent margin lavas can be considered to reflect primary magmas which were in equilibrium with

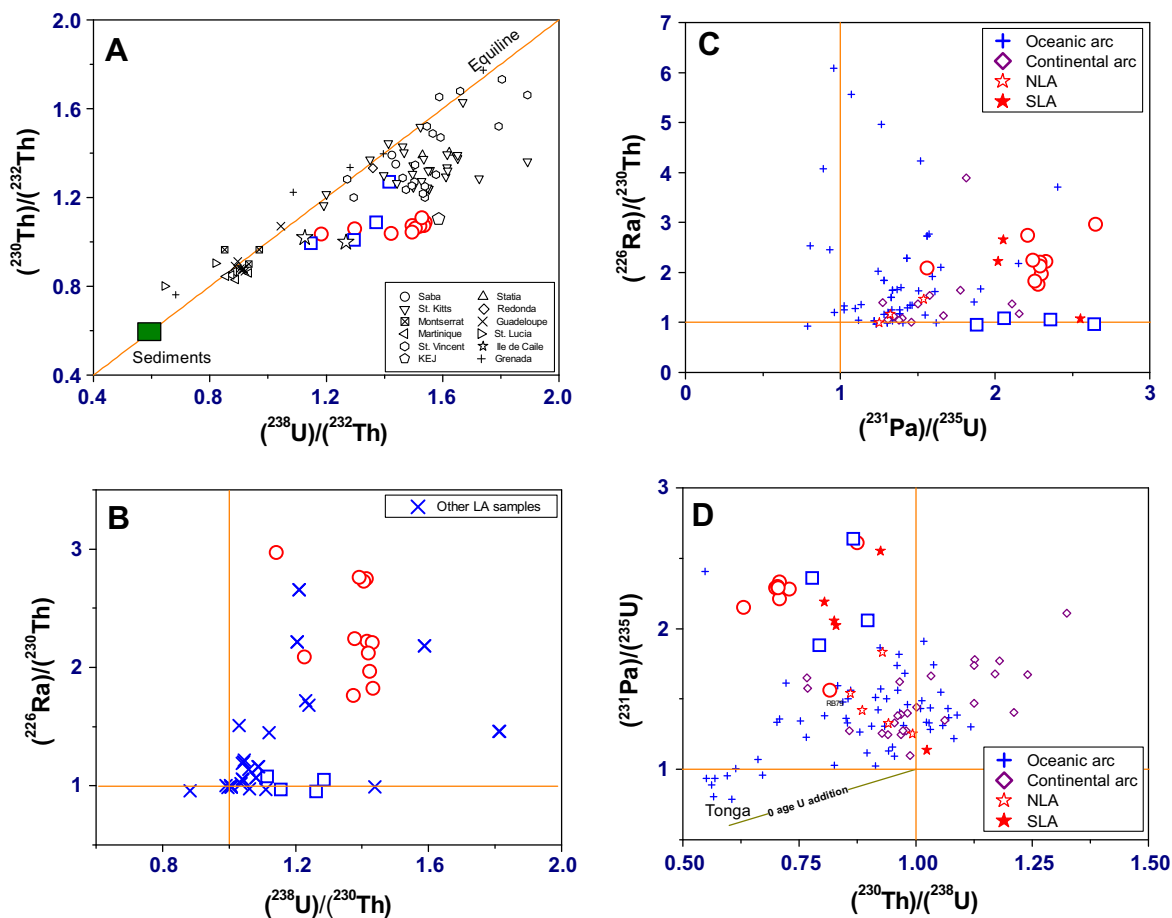


Fig. 5. (A) Comparison of the KEJ samples with lavas from the Lesser Antilles (LA) on a $(^{230}\text{Th})/(^{232}\text{Th})$ – $(^{238}\text{U})/(^{232}\text{Th})$ equiline diagram. Sediment composition is from Plank and Langmuir (1998). Data source for the Lesser Antilles lavas: Heath et al. (1998), Chabaux et al. (1999), Zellmer et al. (2003), Touboul et al. (2007), and DuFrane et al. (2009); (B) $(^{226}\text{Ra})/(^{230}\text{Th})$ versus $(^{238}\text{U})/(^{230}\text{Th})$ of the KEJ and other LA samples. Data source is the same with Fig. 4A; (C and D) $(^{231}\text{Pa})/(^{235}\text{U})$ versus $(^{226}\text{Ra})/(^{230}\text{Th})$ and $(^{230}\text{Th})/(^{238}\text{U})$ for global arc lavas. The Northern LA (NLA) and Southern LA (SLA) data are from Pickett and Murrell (1997), Zellmer et al. (2003), Turner et al. (2006); other arc lava data are from Pickett and Murrell (1997), Bourdon et al. (1999), Thomas et al. (2002), Dosseto et al. (2003), Asmerom et al. (2005), Turner et al. (2006) and Huang and Lundstrom (2007). The open circles and squares stand for the KEJ samples with high ^{226}Ra excesses and $(^{226}\text{Ra})/(^{230}\text{Th})$ close to unity, respectively.

mantle peridotite. Indeed, most have undergone significant amounts of fractional crystallization or assimilation, lowering the Mg# and increasing SiO_2 . Variations of SiO_2 content and Mg# in this suite of KEJ samples clearly indicate that all have undergone significant amounts of differentiation. K/Rb is negatively correlated with Sr, which cannot be explained by fractional crystallization of mafic minerals such as amphibole and clinopyroxene. The lack of negative Eu anomaly and the positive correlation between Sr and SiO_2 argue against a major role of plagioclase during closed system differentiation. Therefore, an open system AFC process is required to explain the geochemical variations in the KEJ samples, similar to that proposed to explain differentiation trends from other Lesser Antilles volcanoes (Thirlwall et al., 1996; Defant et al., 2001; Toothill et al., 2007). The negative correlation between SiO_2 and Ho/Sm or Dy/Yb suggests that the crystallizing mineral assemblage contains considerable amphibole (Davidson et al., 2007). Applying a crustal assimilant with appropriate geochemical features and assuming the assimi-

lation to crystallization ratio (r) is 0.2 with amphibole being the main crystallizing phase (80%) (Table 3), the AFC trajectories using KEJ017 as a representative of the parent magma can satisfactorily explain the variations of Sr contents with Ho/Sm and K/Rb in the KEJ samples (Fig. 4) as well as generally reproduce the REE patterns in Fig. 2B. However, we emphasize that the primitive magma, crystallizing assemblage, and assimilant are poorly constrained, such that the purpose of these models is to show that matches to observed data can be obtained from reasonable assimilants and phase assemblages making AFC a self-consistent although not unique explanation.

5.2. The effect of AFC process on U-series disequilibria in the KEJ lavas

Because the U-series nuclides in most rock forming minerals are highly incompatible (e.g., Blundy and Wood, 2003), it is commonly thought that U-series disequilibria are not significantly affected by fractional crystallization processes

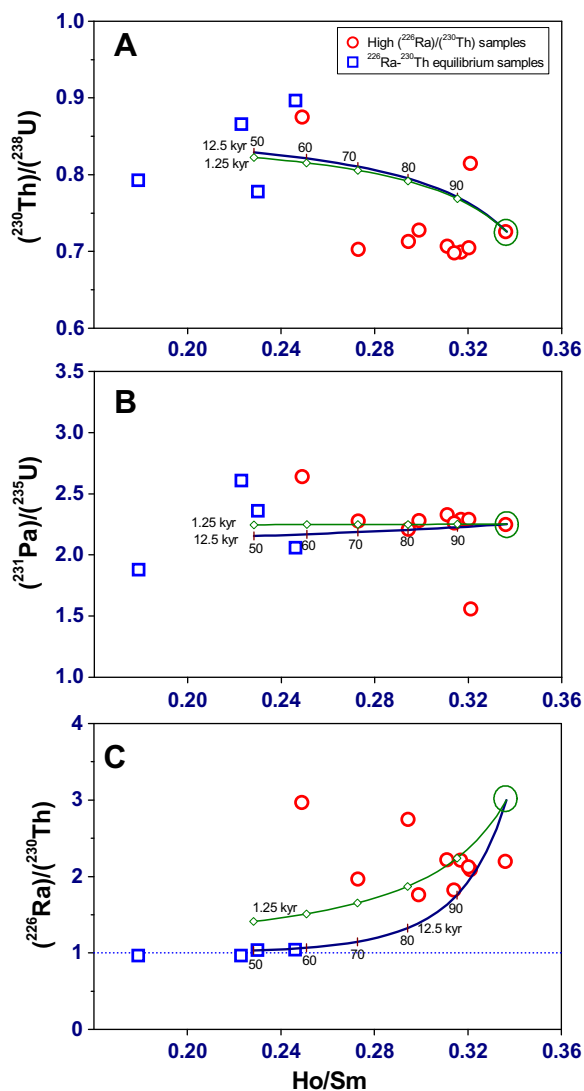


Fig. 6. (A, B, and C) Variations of Ho/Sm with $(^{230}\text{Th})/(^{238}\text{U})$, $(^{231}\text{Pa})/(^{235}\text{U})$, and $(^{226}\text{Ra})/(^{230}\text{Th})$ for the KEJ samples in this study. Also shown are the results of the time-dependent AFC model using the equations in Huang et al. (2008). Fraction of magma remaining (F) is marked in percentage (%). Parameters for the AFC model are from Table 3. The ratio of assimilation rate (r_a) over crystallization rate (r_c) is 0.2. Residence time is $1/(r_c - r_a)$. Because variation of U-series disequilibria during magma differentiation is mainly due to the ageing effect and the geochemical properties of the assimilant (Huang et al., 2008), assuming melt-mineral partition coefficients for Pa of zero does not significantly change the model result.

(e.g., Turner et al., 2003). However, recent numerical models show that assimilating old crustal material along with ageing can significantly modify U-series disequilibria of magmas (Blake and Rogers, 2005; Touboul et al., 2007; Huang et al., 2008). Therefore, the effect of magma differentiation on U-series disequilibria in the KEJ samples needs to be assessed before the disequilibria can be used to constrain the time scales of slab-to surface transfer.

An important observation is that KEJ samples with high $(^{226}\text{Ra})/(^{230}\text{Th})$ have higher Ho/Sm than those with

^{226}Ra – ^{230}Th near equilibrium, while $(^{231}\text{Pa})/(^{235}\text{U})$ in both types of samples are similar (Fig. 6). The difference in Ho/Sm is unlikely to reflect an addition of a slab derived Ra-rich fluid because Ho and Sm are essentially fluid-immobile. As mentioned above, the coherent changes in the REE pattern with SiO_2 contents suggest that the variation in Ho/Sm mostly reflects crustal level differentiation via amphibole fractionation. Therefore, to first order, the relationship between Ho/Sm and $(^{226}\text{Ra})/(^{230}\text{Th})$ should reflect magma differentiation processes. As illustrated in Fig. 6, time-dependent magma differentiation can generally reproduce the features of near equilibrium ^{226}Ra – ^{230}Th and low Ho/Sm in the evolved samples from a less-differentiated magma having higher ^{226}Ra excess and Ho/Sm. While highly simplified, this time-dependent AFC model still usefully shows the possible effects of magma differentiation on U-series disequilibria. Less differentiated samples have similar ^{231}Pa excess and slightly lower $(^{230}\text{Th})/(^{238}\text{U})$ relative to more differentiated samples, suggesting that the AFC process effects these disequilibria little (for ^{230}Th – ^{238}U) to none (for ^{231}Pa – ^{235}U). The simplest interpretation is that the ageing effect is negligible for ^{238}U – ^{230}Th and ^{235}U – ^{231}Pa but significant for ^{226}Ra – ^{230}Th data.

Coupled variations in Sr/Th, Ba/Th, and ^{226}Ra excess in arc lavas have often been regarded to reflect fluid addition processes (e.g., George et al., 2004 and references therein). The large variations of Sr/Th and Ba/Th in low SiO_2 (~50 wt.%) arc lavas indeed require contribution of slab components to the mantle wedge, while decreases in Sr/Th and Ba/Th with increasing SiO_2 must be attributable to magma differentiation (Fig. 3A and B). Notably, $(^{226}\text{Ra})/(^{230}\text{Th})$ of global arc lavas also decreases with increasing SiO_2 (Fig. 3E), leading Huang et al. (2008) to propose that time-dependent AFC processes could alternatively explain the correlations between Sr/Th, Ba/Th, and $(^{226}\text{Ra})/(^{230}\text{Th})$.

Our arguments for differentiation creating these correlations rather than fluid addition follow these lines. If the ^{226}Ra excess in KEJ lavas were from fluid addition, the positive correlations should be more clearly observed in the less evolved samples with higher Mg#. As shown in Fig. 7, the four samples with both high Mg# (>60) and ^{226}Ra excess have variable Sr/Th (225–139) and Ba/Th (85–65), but nearly constant $(^{226}\text{Ra})/(^{230}\text{Th})$ (2.09–2.22); no correlation with Sr/Th and Ba/Th is apparent. In contrast, for the low Mg# (<60) samples, $(^{226}\text{Ra})/(^{230}\text{Th})$ correlates well with Sr/Th and Ba/Th, fully consistent with the time-dependent AFC process proposed by Huang et al. (2008). Furthermore, the samples with ^{226}Ra – ^{230}Th close to equilibrium have lower Ho/Sm which for KEJ samples is an index of greater degrees of differentiation. While we do not dispute that Sr, Ba, Ra, and other fluid-mobile elements are added to the mantle wedge at the slab–wedge interface, there is no evidence supporting the ^{226}Ra excess observed in KEJ lavas being produced by this process.

5.3. The role of in-growth melting in generating U-series disequilibria in subduction zones

Because of the greater mobility of U and Ra relative to Th in hydrous fluids having higher $f\text{O}_2$ or salinity (Keppler

Table 3

Partition coefficients and concentrations of trace elements and U-series nuclides (ppm) in the initial magma and assimilant.

	Rb	K	Ba	Sr	La	Ce	Pr	Nd	Sm	Eu	Gd	Tb	Dy	Ho	Er	Tm	Yb	Lu
Plg/melt D	0.010	0.050	0.264	2.360	0.072	0.055	0.055	0.043	0.039	0.258	0.038	0.025	0.029	0.020	0.018	0.010	0.010	0.007
Cpx/melt D	0.001	0	0	0.063	0.099	0.158	0.237	0.335	0.535	0.621	0.697	0.758	0.800	0.818	0.817	0.802	0.778	0.748
Amph/melt D	0.2	0.58	0.16	0.298	0.116	0.185	0.277	0.396	0.651	0.657	0.933	1.00	0.967	1.03	0.851	0.816	0.787	0.698
Bulk D	0.161	0.47	0.156	0.481	0.025	0.039	0.066	0.106	0.222	0.310	0.358	0.425	0.487	0.529	0.555	0.563	0.560	0.548
Initial magma	14.2	4232	95	172, 266	4.11	9.53	1.40	6.98	2.25	0.85	2.90	0.53	3.55	0.76	2.02	0.29	1.83	0.29
Assimilant	142.9	11900	829	638	52.18	91.56	9.40	30.23	4.64	1.39	3.82	0.57	3.08	0.62	1.79	0.39	1.97	0.34
	U	Th	Pa	Ra	(²³⁸ U)/(²³² Th)	(²³⁰ Th)/(²³² Th)	(²³⁸ U)/(²³⁰ Th)	(²²⁶ Ra)/(²³⁰ Th)	(²³¹ Pa)/(²³⁵ U)									
Plg/melt D	0.0006	0.003	0	0.0304														
Cpx/melt D	0.002	0.0029	0	0														
Amph/melt D	0.0041	0.0039	0	0.0128														
Bulk D	0.00354	0.00376	0	0.0133														
Initial magma	0.58	1.15	4.24 × 10 ⁻⁷	4.25 × 10 ⁻⁷	1.53		1.11		1.377		3		2.25					
Assimilant	10.16	26.80	7.43 × 10 ⁻⁶	2.97 × 10 ⁻⁶	1.15		0.994		1.155		1		2.25					

Plagioclase, plg; clinopyroxene, cpx; amphibole, amph. $^{Plg/melt}D$ are from (Bindeman et al., 1998; Zajacz and Halter, 2007); $^{Cpx/melt}D_{REE}$ are from experiment 4EHE in Hill et al. (2000). $^{Cpx/melt}D$ for U, Th, and Sr are from experiment Tr9 in Lundstrom et al. (1994). $^{Cpx/melt}D$ for K and Ba are zero. $^{Amph/melt}D$ for Rb, K, Ba, and Sr from Latourrette et al. (1995), and REEs from Bottazzi et al. (1999). $^{Amph/melt}D_{Ra}$ is calculated from Blundy and Wood (2003), while $^{Plg/melt}D_{Ra}$ is calculated from Eq. (6) in Fabbriozio et al. (2009) assuming $X_n = 0.65$ and $T = 1050$ °C. D_{Pa} for all minerals is zero, which does not significantly change the result of the AFC model. Bulk $D = ^{Amph/melt}D \times 0.8 + ^{Plg/melt}D \times 0.1 + ^{Cpx/melt}D \times 0.1$. (²²⁶Ra)/(²³⁰Th) of the initial magma and assimilant is 3 and 1, respectively. The initial magma uses variable Sr contents to account for the heterogeneity of primitive magma. Curve 1 in Fig. 7A uses Sr of 172 ppm and Sr/Th of 150, while curve 2 uses the Sr and Th contents of KEJ017. Other trace element and U-series data for the initial magma use the data of the most primitive sample, KEJ017. Trace element compositions except U of the assimilant are calculated assuming the assimilant is a 40% batch melt of the most differentiated sample RB47 with 80% amphibole, 10% clinopyroxene, and 10% plagioclase as the solidus phases. U/Th and (²³⁰Th)/(²³²Th) of the assimilant are from Rb65. Because (²³¹Pa)/(²³⁵U) does not vary with differentiation indices, (²³¹Pa)/(²³⁵U) of the assimilant and primitive magma are fixed at 2.25.

and Wyllie, 1990; Keppler, 1996; Bali et al., in press), excesses of ²³⁸U and ²²⁶Ra over ²³⁰Th in arc lavas are most often attributed to the process of hydrous fluid addition from the slab (Turner et al., 2003 and references therein). If so, then the time scale from the time of slab fluid addition to eruption must be <8000 yrs, placing tight constraints on magma ascent velocities (e.g., Turner et al., 2000, 2001, 2003; George et al., 2003, 2004). Yet the large ²³¹Pa excesses over ²³⁵U observed in many arc settings provide a contradiction to this simple model of fluid addition. If Pa, as a HFSE element, has similar immobility to Th and Nb, then an excess of ²³⁵U should occur over ²³¹Pa. However, ²³⁵U excess is extremely rare, having been observed in only a few samples from Tonga and Kermadec to date (Bourdon et al., 1999).

Indeed, ²³¹Pa excesses are ubiquitously observed in young magmas in all tectonic settings including convergent margins (e.g., Pickett and Murrell, 1997; Bourdon and Sims, 2003 and references therein; Dosseto et al., 2003; Lundstrom, 2003 and references therein; Turner et al., 2006). A key point to make is that if in-growth melting processes (based on differing residence times of U and Pa in the melting column) produce the ²³¹Pa–²³⁵U disequilibria as has been suggested by numerous workers (Pickett and Murrell, 1997; Thomas et al., 2002; Dosseto et al., 2003; Turner et al., 2006; Huang and Lundstrom, 2007), then disequilibria between all other U-series parent–daughter pairs having differing $^{solid/melt}D$ must also be produced during

this process. For instance, any in-growth based process forming (conservatively) 100% excess of ²³¹Pa requires a ²³⁵U residence time of order the half life of ²³¹Pa, or 32.8 kyr. Therefore, any ²²⁶Ra excess produced at the slab but participating in the melt generation process cannot survive the melting column residence time dictated by the ²³¹Pa. Only if a multi-stage fluid addition process occurs to add ²²⁶Ra independently of melting could the signature be preserved; even then it would be subject to mixing with the ²²⁶Ra–²³⁰Th produced in the melting column.

Below we use a series of in-growth melting models to reproduce U-series disequilibria of the KEJ samples, including the inclined linear trend between (²³⁰Th)/(²³²Th) and (²³⁸U)/(²³²Th) on the U–Th equiline diagram, the high ²³¹Pa excesses coexisting with high (²³⁸U)/(²³⁰Th), and the ²²⁶Ra excesses.

5.3.1. The inclined linear trend between (²³⁰Th)/(²³²Th) and (²³⁸U)/(²³²Th)

Linear trends on the U–Th equiline diagram between (²³⁰Th)/(²³²Th) and (²³⁸U)/(²³²Th) have been observed in several subduction zones including New Britain (Gill et al., 1993), Mariana (Elliott et al., 1997), Vanuatu (Turner et al., 1999), and the Aegean (Zellmer et al., 2000). While such trends have been most commonly interpreted to reflect the time of decay since addition of U-rich fluid to the mantle wedge (Elliott et al., 1997), alternative explanations also exist for this observation. For instance, addition of a U-rich

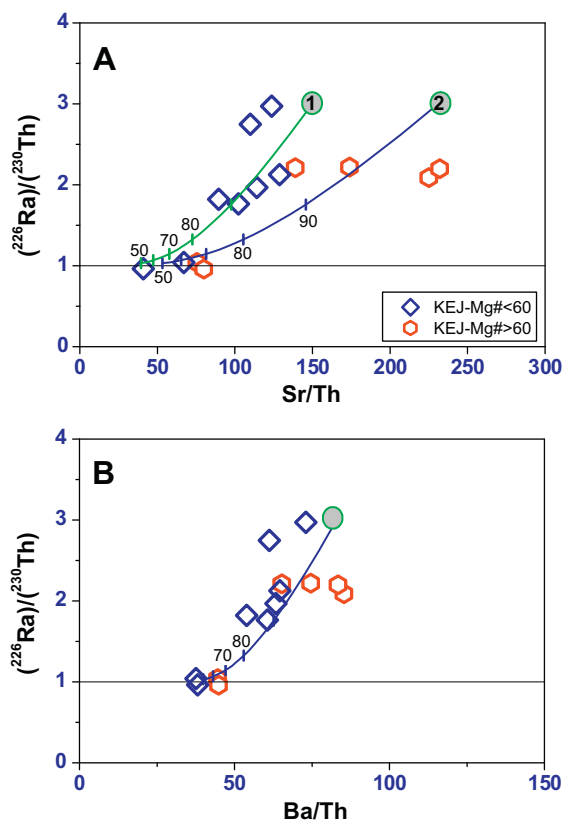


Fig. 7. (A and B) Simulations of the positive correlations of $(^{226}\text{Ra})/(^{230}\text{Th})$ with Sr/Th and Ba/Th in the KEJ samples using the time-dependent AFC model (Huang et al., 2008). Fraction of magma remaining (F) is marked in percentage (%). The AFC model use parameters from Table 3 and assume r_a/r_c is 0.2 and residence time is 12.5 kyr. Sr/Th and Ba/Th for the KEJ samples are from Tables 1 and 2.

fluid with variable amounts of Th to a homogenous mantle source or a constant addition of U-rich fluid to the wedge

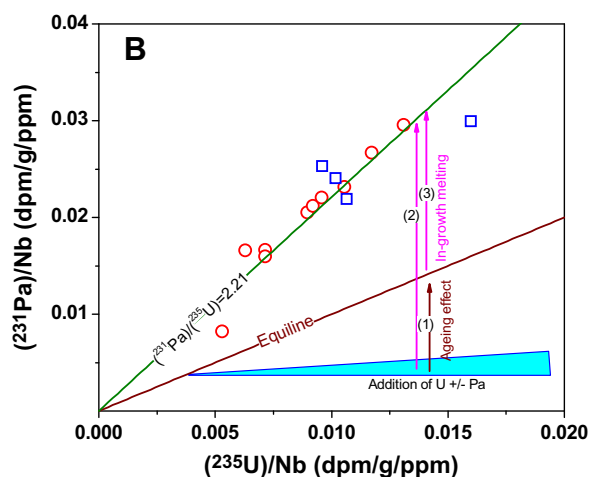
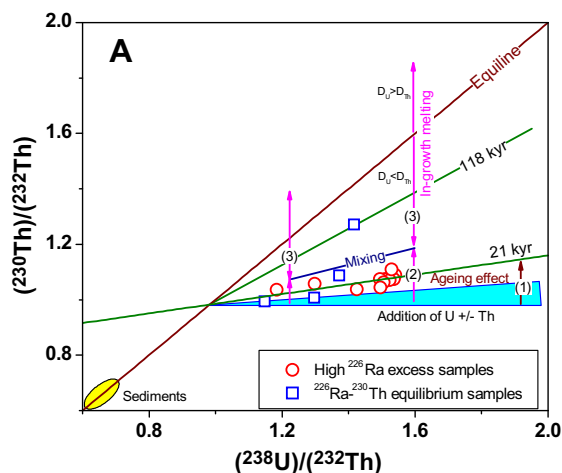


Fig. 8. “Isochron” diagrams of (A) $(^{230}\text{Th})/(^{232}\text{Th})$ versus $(^{238}\text{U})/(^{232}\text{Th})$ and (B) $(^{231}\text{Pa})/\text{Nb}$ versus $(^{235}\text{U})/\text{Nb}$. The slope of an isochron line is $1 - e^{-\lambda t}$, where λ is the decay constant of ^{230}Th or ^{231}Pa . Arrow (1) stands for ageing (or decay) effect on the mantle source with recent U-addition, while (2) and (3) stand for in-growth melting of the mantle source with and without U-series disequilibrium, respectively. In (A), the left and right arrow 3 have the same $^{230}\text{Th}/^{238}\text{U}$ constraints varying from >1 to <1 due to increasing $f\text{O}_2$.

with variable U/Th, and dynamic melting of a source with ^{238}U excess have also been invoked (Elliott et al., 1997; George et al., 2003; Turner et al., 2003 and references therein). The KEJ samples excepting KEJ103 define a line that could represent a 21 kyr isochron, assuming simple horizontal U-Th fractionation followed by ageing (arrow (1) in Fig. 8A). However, the high ^{231}Pa excesses observed rule out this interpretation because the time-scale required for enough ^{231}Pa in-growth should be much longer than 21 kyr and a simple parent–daughter fractionation and ageing effect cannot explain the ^{231}Pa excess. Instead, an in-growth melting process (involving a source with a ^{231}Pa -deficit (arrow (2) in Fig. 8B) or in ^{235}U – ^{231}Pa equilibrium (arrow (3) in Fig. 8B)) is required to produce the ^{231}Pa excesses and this process will also affect the ^{238}U – ^{230}Th disequilibria as illustrated by our modeling.

While in-growth melting processes are always invoked for explaining ^{231}Pa excesses, this interpretation has not often been integrated with the ^{238}U – ^{230}Th and ^{226}Ra – ^{230}Th observations in arc lavas. For instance, if ^{231}Pa excess is generated by a longer residence time of ^{235}U in the melting column, then the same residence time will apply to ^{238}U and thus also affect ^{230}Th – ^{238}U . Only if $^{230}\text{Th}/^{238}\text{U}$ were coincidentally identical to $^{231}\text{Pa}/^{235}\text{U}$ would this process have no effect on ^{230}Th – ^{238}U disequilibrium. Experimental studies on partition coefficients of U and Th between mantle minerals and silicate melt have shown that $^{230}\text{Th}/^{238}\text{U}$ is strongly dependant on oxygen fugacity ($f\text{O}_2$), decreasing from >1 to <1 with increasing $f\text{O}_2$ (e.g., Beattie, 1993; Lundstrom et al., 1994) and this could play an important role in the generation of ^{238}U – ^{230}Th disequilibria during melting (Huang and Lundstrom, 2007). Arrow (3) in Fig. 8A shows that when $^{230}\text{Th}/^{238}\text{U} > 1$, in-growth melting of a source in secular equilibrium results in ^{230}Th excesses over ^{238}U similar to those found in MORB (e.g., Lundstrom, 2003), ocean island basalts (e.g., Bourdon and Sims, 2003), and some continental arc lavas (e.g., Turner et al., 2003). However, in an oxidized mantle wedge

(Parkinson and Arculus, 1999) or in spinel lherzolite at shallow depths (Tepley et al., 2004) where $D_{U/Th}^{solid/melt} < 1$, ^{238}U excesses are produced by in-growth melting of the mantle source regardless of the initial ^{238}U excess as shown by arrow (2) and (3) in Fig. 8A. Therefore, theoretically, if the time-scale of mantle melting is long enough, whether ^{238}U excesses are initially created at the slab interface makes no difference as the melting process occurring in the overlying melting column controls the ^{238}U excesses that are observed in most arc lavas.

One caveat to this conclusion is that ^{238}U – ^{230}Th or even ^{231}Pa – ^{235}U developed at the slab–wedge interface could still be important in the specialized case of arcs having high convergence rates and melting rates (e.g., Tonga). Because the melting rate is low in a slow subduction zone due to the decreased water reaching the melting area (Cagnioncle et al., 2007; Huang and Lundstrom, 2007), the effect of residence time based partial melting on U-series disequilibria is more prominent in the Southern Lesser Antilles than in a fast subduction zone. Therefore, although the Southern Lesser Antilles arc is special in terms of the great contribution of sediment composition to the mantle wedge, the initial U-series disequilibria in the mantle wedge produced by adding fluid or sediment should not significantly affect the disequilibria observed in the KEJ samples. For the purpose of demonstrating an end-member model, where U-series disequilibria are solely produced by in-growth melting, we simply assume that the mantle wedge beneath the Southern Lesser Antilles arc is in U-series secular equilibrium prior to partial melting. In this regard, adding Th or U bearing fluids to the mantle source is not further considered for explaining the linear trend between $(^{230}Th)/(^{232}Th)$ and $(^{238}U)/(^{232}Th)$.

Both flux melting and adiabatic decompressional melting can occur in the mantle wedge at arcs (e.g., Cagnioncle et al.,

2007). A number of in-growth melting models have been proposed to explain U-series disequilibria in young arc lavas. These models include dynamic melting (DM) (Bourdon et al., 2003; Dosseto et al., 2003; Turner et al., 2003, 2006), flux melting (FM) (Thomas et al., 2002; Bourdon et al., 2003), and reactive porous flow (RPF) (Spiegelman and Elliott, 1993; Turner et al., 2006; Huang and Lundstrom, 2007); all can generally reproduce U-series disequilibria in arc lavas with appropriate parameters applied including a large variation of U/Th in the mantle source (Table 4 and Fig. 9). We vary $D_{U/Th}^{solid/melt}$ but keep $D_{Th}^{solid/melt}$ constant to assess the effect of fO_2 variations on ^{238}U – ^{230}Th disequilibrium. These models are essentially similar to the one used in Beier et al. (2010) where in-growth melting of an oxidized and heterogeneous mantle was called upon to explain the ^{238}U and ^{226}Ra excesses in the Manus Basin lavas ~150 km behind the New Britain volcanic arc.

The results of three in-growth models consistently show that, if $D_{U/Th}^{solid/melt}$ is higher than $D_{Th}^{solid/melt}$ at low fO_2 , ^{230}Th excess can be produced, while decreasing $D_{U/Th}^{solid/melt}$ leads to increasing $(^{238}U)/(^{230}Th)$, producing significant ^{238}U excesses over ^{230}Th in the melt when $D_{U/Th}^{solid/melt} < 1$ (Fig. 9). In Fig. 9A, the KEJ data define a shallower slope than the grid lines of models using different U/Th but similar $D_{U/Th}^{solid/melt}$. This may be due to overestimating $D_{U/Th}^{solid/melt}$ for a source with high U/Th. As shown in a recent experimental study, increasing fO_2 not only decreases $D_{U/Th}^{solid/melt}$, but also enhances the fluid mobility of U but not Th (Bali et al., in press). Therefore, a high U/Th source is more likely coupled with a low $D_{U/Th}^{solid/melt}$ in the modeling. Based on the results of in-growth melting models, we propose that an alternative explanation for the inclined linear trend in U–Th equiline diagram could be mixing between two melts derived from heterogeneous mantle sources with variable U/Th

Table 4

Parameters used in in-growth melting models. Partition coefficient data are from Blundy and Wood (2003) and the compilation in Turner et al. (2006). Bulk partition coefficients are calculated only using olivine and pyroxene data.

Partition coefficients	Olivine	Orthopyroxene	Clinopyroxene	Spinel	Bulk
Mineral mode	52	28	17	3	
D_U	6.0×10^{-5}	7.8×10^{-3}	1.8×10^{-2}	$<10^{-5}$	5.2×10^{-3}
D_{Th}	9.5×10^{-5}	3.0×10^{-3}	2.1×10^{-2}	$<10^{-5}$	4.4×10^{-3}
D_{Pa}	6.0×10^{-8}	7.8×10^{-6}	1.8×10^{-9}	0	2.1×10^{-6}
D_{Ra}	5.8×10^{-8}	6.0×10^{-7}	4.1×10^{-6}	0	8.9×10^{-7}
Physical parameters	Unit	Value	Comments		
Melt density, ρ_m	kg/m ³	2800			
Solid density, ρ_s	kg/m ³	3340			
Melt degree, F	–	0.1			
Porosity, ϕ	–	0.002			
Amount of convergence, d	km	90			
Subduction rate, v_s	cm/yr	1.3			From Speed et al. (1993)
Matrix velocity, W	cm/yr	–			Assuming $W = v_s$
Melting rate, Γ	kg/m ³ /yr	–			$\Gamma = F\rho_s v_s/d$

Fluid composition per increment (ppm) in flux melting models (Thomas et al., 2002)

dU/dF	$d^{232}Th/dF$	$d^{230}Th/dF$	dPa/dF	dRa/dF
0.2	4.07×10^{-2}	9.83×10^{-7}	3.38×10^{-8}	2.04×10^{-6}

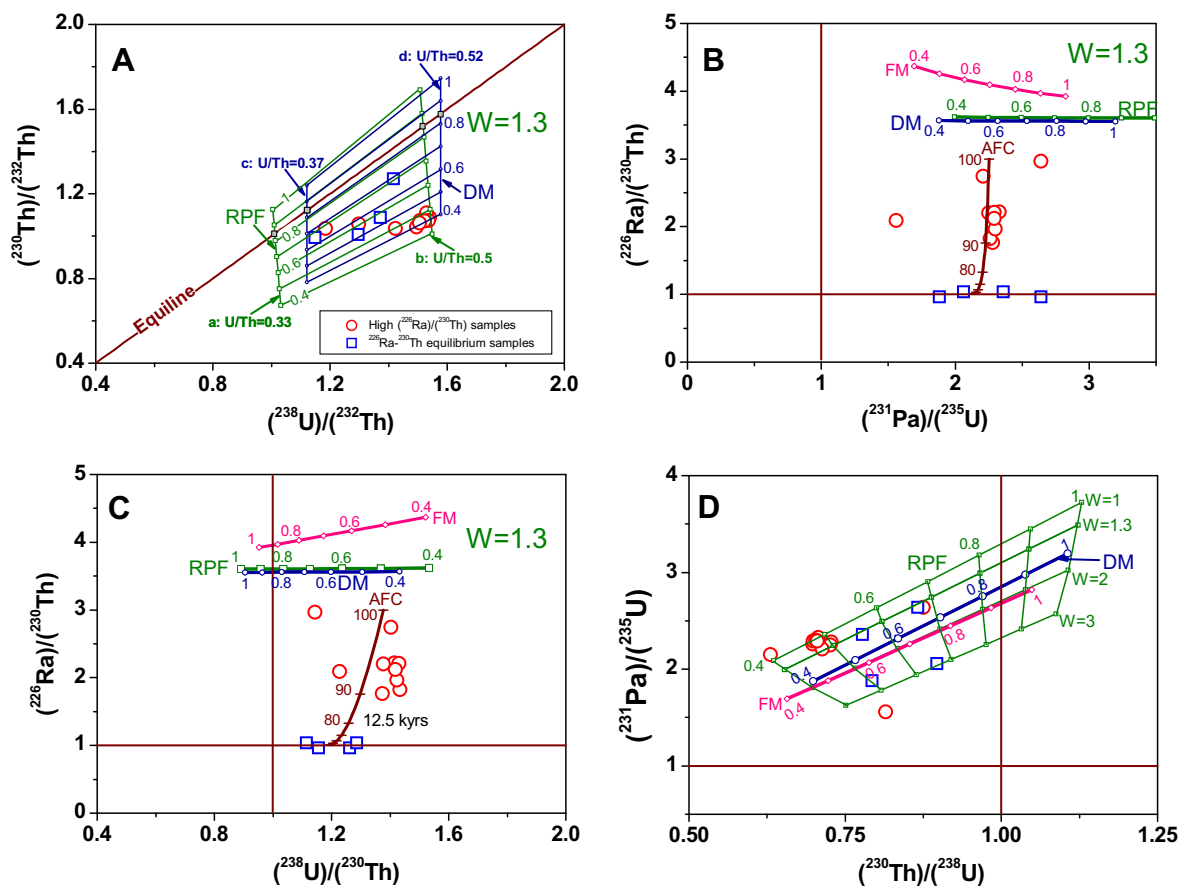


Fig. 9. (A), Grids using the reactive porous flow (RPF) and dynamic melting (DM) models show the effect of in-growth melting of the heterogeneous mantle source within ^{238}U – ^{230}Th equilibrium. The DM calculation uses equations in Williams and Gill (1989) and RPF follows the equations in Spiegelman and Elliott (1993). Parameters used in the models are given in Table 4. Partition coefficients of Th, Pa, and Ra are assumed to be constant, while D_{U} decrease from the initial $D_{\text{U}}(0)$ (0.0052) due to the high $f\text{O}_2$ in the wedge. The model results are contoured for U/Th in the source and $D_{\text{U}}/D_{\text{U}}(0)$. (B) and (C), $(^{226}\text{Ra})/(^{230}\text{Th})$ versus $(^{238}\text{U})/(^{230}\text{Th})$ and $(^{231}\text{Pa})/(^{235}\text{U})$ diagrams showing how in-growth melting processes produce U-series disequilibria, which are modified by the later time-dependent AFC process. The flux melting (FM) model is from Thomas et al. (2002) using the melting rate calculated in Table 4. The bulk D for U is also varied during the calculation based on variation of $f\text{O}_2$. (D), $(^{230}\text{Th})/(^{238}\text{U})$ versus $(^{231}\text{Pa})/(^{235}\text{U})$ diagram showing the effects of in-growth melting. The RPF model is contoured for subduction rate (i.e., matrix velocity) and $D_{\text{U}}/D_{\text{U}}(0)$. The melting rate for the DM and FM models is also similar to (A) assuming the matrix velocity is 1.3 cm/yr. All in-growth melting models assume the source is in U-series equilibrium. The AFC model in (B–D) used parameters in Table 3 and a residence time of 12.5 kyr with the fraction of magma remaining marked in percentage (%). The numbers near the three in-growth melting models stand for the ratio of a decreased $D_{\text{U}}^{\text{solid/melt}}$ (due to increasing $f\text{O}_2$) over the initial unmodified $D_{\text{U}}^{\text{solid/melt}}(0)$ (i.e., $D_{\text{U}}/D_{\text{U}}(0)$).

and $f\text{O}_2$. This mixing process could accompany magma differentiation in the shallow crust as discussed above. We do agree that significant fractionation of U and Th may occur at the slab–wedge interface and this is likely to produce the variation in U/Th observed; however, such elemental fractionation does not imply that ^{238}U – ^{230}Th disequilibrium created by this process is preserved in erupted lavas.

5.3.2. Coexistence of high ^{231}Pa excesses with high ^{238}U excesses

KEJ provides an interesting case study as it combines the highest ^{231}Pa excesses in arcs globally with large ^{238}U excesses. However, the coexistence of high ^{231}Pa and ^{238}U excesses is not unique in global arc lavas. Lavas from nearby volcanoes in the Southern Lesser Antilles (e.g.,

St. Vincent and Ile de Caile) (Turner et al., 2006), Ija in Sunda (Turner et al., 2006), and Vesuvius in southern Italy (Avanzinelli et al., 2007) are also characterized by having similar features. Given that the majority of young oceanic arc lavas have ^{238}U excesses and ^{231}Pa excesses (Fig. 5D), understanding the generation of combined high ^{231}Pa and ^{238}U excesses may provide important insights into rates of slab-flux transfer and partial melting of the mantle wedge.

Globally, there is no simple positive correlation between $(^{230}\text{Th})/(^{238}\text{U})$ and $(^{231}\text{Pa})/(^{235}\text{U})$ in arc lavas if the Southern Lesser Antilles samples are included. Instead, the global dataset can be divided into three end-member groups which can be represented by the Southern Lesser Antilles (with high ^{231}Pa and ^{238}U excesses), Tonga (with high

^{238}U excesses but low ^{231}Pa excesses or deficits), and some continental arcs (with ^{230}Th and ^{231}Pa excesses), respectively (Fig. 5D). As an end-member arc, the Southern Lesser Antilles has the slowest subduction rate and highest ^{231}Pa excesses, while the Tonga arc, the other end-member, has the fastest subduction rate and lowest $(^{231}\text{Pa})/(^{235}\text{U})$. If the melting rate of the mantle mainly reflects the water flux added from the subducted slab, and thus is a linear function of subduction rate (Huang and Lundstrom, 2007), in-growth melting processes at low melting rates could produce the high ^{231}Pa excesses regardless of the initial $(^{231}\text{Pa})/(^{235}\text{U})$ (≤ 1). As mentioned above, the ^{238}U excesses could also be due to in-growth melting of the mantle wedge with or without initial ^{238}U excesses from the slab if $^{\text{solid/melt}}D_{\text{U/Th}}$ in the melting column is less than 1. As shown in Fig. 9D, the results of the RPF model using various matrix velocities and values for $^{\text{solid/melt}}D_{\text{U/Th}}$ are generally consistent with the $(^{231}\text{Pa})/(^{235}\text{U})$ versus $(^{230}\text{Th})/(^{238}\text{U})$ trend. The FM and DM models can also reproduce the KEJ trend with appropriate parameters applied. For the case of Tonga, while the observation of $(^{231}\text{Pa})/(^{235}\text{U}) < 1$ in a few samples requires a recent U-rich flux to the mantle wedge (Bourdon et al., 1999), many of the Tonga samples have slight ^{231}Pa excess, suggesting that in-growth melting overprints the initial ^{231}Pa deficit of the source (Bourdon et al., 1999; Turner et al., 2006). For some continental arc lavas, in-growth melting with garnet or Al-rich clinopyroxene as residual mineral(s) best explains ^{230}Th and ^{231}Pa excesses (Wood et al., 1999; Blundy and Wood, 2003). The majority of arc lavas have combined ^{238}U and ^{231}Pa excesses (but with smaller excess compared to KEJ), similarly reflecting the effect of in-growth melting of the heterogeneous mantle wedge with the variable initial U-series daughter–parent ratios, U/Th, $f\text{O}_2$, and melting rate (as a function of a physical, thermal and petrologic parameters such as subduction rate, mantle potential temperature, and slab water content).

5.3.3. ^{226}Ra excesses in arc lavas

In-growth melting processes in the mantle (McKenzie, 1985; Spiegelman and Elliott, 1993) have been called upon to explain ^{226}Ra – ^{230}Th , ^{231}Pa – ^{235}U , and ^{238}U – ^{230}Th disequilibria within “dry” tectonic settings such as MORB (e.g., Lundstrom, 2003 and references therein) and OIB (e.g., Bourdon and Sims, 2003 and references therein). However, such processes have not been invoked to explain ^{226}Ra excesses in arc lavas because they cannot readily explain the positive correlations between ^{226}Ra excesses and Sr/Th or Ba/Th. In order to reconcile the ^{231}Pa excesses with ^{226}Ra excesses in arc lavas, many authors have proposed that in-growth of ^{231}Pa is followed by rapid melt extraction in order to preserve ^{226}Ra excesses produced by Ra-rich fluid addition (Thomas et al., 2002; Bourdon et al., 2003; Dosseto et al., 2003; Turner et al., 2003, 2006). However, because any in-growth melting process will produce ^{226}Ra excess during the time it produces ^{231}Pa and ^{238}U excesses, a later, second stage ^{226}Ra -rich fluid addition from the slab is not needed to explain the creation of ^{226}Ra excesses.

Based on the discussion above, we propose the alternative explanation that ^{226}Ra excesses in arc lavas mostly reflect in-growth processes during melting (e.g., either in-growth melting or diffusion based melting and reaction) (Feineman and DePaolo, 2003; Van Orman et al., 2006; Huang and Lundstrom, 2007) and do not simply reflect slab fluid transfer and rapid ascent. This is consistent with the general observation of large ^{231}Pa and ^{226}Ra excesses in many subduction zone lavas (e.g., Dosseto et al., 2003; Turner et al., 2006; Huang and Lundstrom, 2007); furthermore, evidence supporting the fluid addition process can better be explained by the positive correlations between ^{226}Ra excess and Ba/Th and Sr/Th resulting from time-dependent magma differentiation at shallow crustal depths (Huang et al., 2008). This conclusion leads to relaxing the temporal constraints on magma ascent inferred by ^{226}Ra excesses. If this conclusion is applicable to the global arc settings, the time-scales for slab-flux transfer and magmatism in convergent margins are no longer constrained to be < 8000 yrs and are probably more similar to the half-lives of ^{231}Pa (32.8 kyr) or ^{230}Th (75.7 kyr).

6. CONCLUSIONS

Lavas from KEJ submarine volcano in the Southern Lesser Antilles arc have high ^{231}Pa excesses over ^{235}U as well as high ^{238}U and ^{226}Ra excesses over ^{230}Th . The high ^{231}Pa excesses are best explained by in-growth melting processes occurring in the mantle wedge in a low convergence rate setting. This in-growth melting process can also explain the high ^{238}U and ^{226}Ra excesses if $^{\text{solid/melt}}D_{\text{U/Th}} < 1$ in the oxidizing mantle wedge. Samples with large ^{226}Ra excess have relatively higher Ho/Sm compared with those having ^{226}Ra – ^{230}Th near equilibrium. While $(^{226}\text{Ra})/(^{230}\text{Th})$ follows the commonly observed positive correlation with either Sr/Th or Ba/Th, the relationship with REE data are not consistent with the ^{226}Ra excess simply reflecting fluid addition from the slab. Instead, it more likely reflects an open system magma differentiation process as indicated by the negative correlations of Sr with Ho/Sm and K/Rb.

Given that ^{231}Pa excesses are observed universally among arcs, we propose that in-growth based processes probably play a more important role in producing ^{238}U and ^{226}Ra excesses in arc lavas than previously acknowledged. In-growth melting of a heterogeneous mantle wedge with variable initial conditions (e.g., U/Th and daughter-pair ratios), $f\text{O}_2$, thermal structure, and matrix velocity can account for the disequilibria in ^{238}U – ^{230}Th , ^{230}Th – ^{226}Ra , and ^{235}U – ^{231}Pa observed in convergent margins. Furthermore, the ^{226}Ra – ^{230}Th disequilibria produced by this partial melting process can be significantly modified by the later time-dependent magma differentiation processes, resulting in the correlations between U-series data and many other geochemical parameters (e.g., ^{226}Ra excesses vs. Sr/Th and Ba/Th) and the inclined linear trend between $(^{230}\text{Th})/(^{232}\text{Th})$ and $(^{238}\text{U})/(^{232}\text{Th})$. Therefore, ^{226}Ra excess generation due to recent fluid addition is not needed to explain these correlations and the temporal constraint on magmas going from slab to surface in < 8000 yrs likely needs to be relaxed. Our estimated time-scales of magmatism and flux transfer from the slab

range from tens of thousands years up to < several millions years as constrained from ^{10}Be data in arc lavas (e.g., Sigmarsson et al., 1990, 2002).

ACKNOWLEDGMENTS

Work in the UIUC MC-ICP-MS lab is supported by NSF EAR 0732481. Comments from Ken Sims, Jim Gill, Kari Cooper, and an anonymous reviewer greatly improved this manuscript. We thank the GeoAnalytical Lab of Washington State University (Pullman) for trace element analyses, Mark Reagan for ^{210}Po analyses, and Justin Glessner for help with the U-series analyses. We also thank Marc Hirschmann for providing the spreadsheet for his flux melting model, Joe Devine for generously providing some KEJ samples and comments on an early version of this paper, and Frederick Frey for editorial handling. Discussion with Alistair Hack is gratefully acknowledged.

REFERENCES

- Asmerom Y., DuFrane S. A., Mukasa S. B., Cheng H. and Edwards R. L. (2005) Time scale of magma differentiation in arcs from protactinium–radium isotopic data. *Geology* **33**, 633–636.
- Avanzinelli R., Prytulak J., Elliott T., Mattei M. and Conticelli S. (2007) Metasomatism and melting in subduction-related volcanics: U–Th–Pa constraints from Vesuvius. In *Goldschmidt Conference Abstracts*.
- Bali E., Audétat A. and Keppler H. (in press) The mobility of U and Th in subduction zone fluids: an indicator of oxygen fugacity and fluid salinity. *Contrib. Mineral. Petrol.*
- Beattie P. (1993) Uranium–thorium disequilibrium and partitioning on melting of garnet peridotite. *Nature* **363**, 63–65.
- Beier C., Turner S. P., Sinton J. M. and Gill J. B. (2010) Influence of subducted components on back-arc melting dynamics in the Manus Basin. *Geochem. Geophys. Geosyst.* **11**, Q0AC03. doi:10.1029/2010GC003037.
- Berlo K. and Turner S. (2010) ^{210}Pb – ^{226}Ra disequilibria in volcanic rocks. *Earth Planet. Sci. Lett.* **296**, 155–164.
- Bindeman I. N., Davis A. M. and Drake M. J. (1998) Ion microprobe study of plagioclase–basalt partition experiments at natural concentration levels of trace elements. *Geochim. Cosmochim. Acta* **62**, 1175–1193.
- Blake S. and Rogers N. (2005) Magma differentiation rates from ($^{226}\text{Ra}/^{230}\text{Th}$) and the size and power output of magma chambers. *Earth Planet. Sci. Lett.* **236**, 654–669.
- Blundy J. and Wood B. (2003) Mineral–melt partitioning of Uranium, Thorium and their daughters. *Rev. Mineral. Geochem.* **52**, 59–123.
- Bottazzi P., Tiepolo M., Vannucci R., Zanetti A., Brumm R., Foley S. F. and Oberti R. (1999) Distinct site preferences for heavy and light REE in amphibole and the prediction of $^{A_{\text{Amph}}/L_{\text{DREE}}}$. *Contrib. Mineral. Petrol.* **137**, 36–45.
- Bourdon B. and Sims K. (2003) U-series constraints on intraplate basaltic magmatism. *Rev. Mineral. Geochem.* **52**, 215–254.
- Bourdon B., Turner S. and Allègre C. (1999) Melting dynamics beneath the Tonga–Kermadec island arc inferred from ^{231}Pa – ^{235}U systematics. *Science* **286**, 2491–2493.
- Bourdon B., Turner S. and Dosseto A. (2003) Dehydration and partial melting in subduction zones: constraints from U-series disequilibrium. *J. Geophys. Res.* **108**, 2291.
- Chabaux F., Hémond C. and Allègre C. (1999) ^{238}U – ^{230}Th – ^{226}Ra disequilibria in the Lesser Antilles arc: implications for mantle metasomatism. *Chem. Geol.* **153**, 171–185.
- Cagnioncle A., Parmentier E. M. and Elkins-Tanton L. T. (2007) Effect of solid flow above a subducting slab on water distribution and melting at convergent plate boundaries. *J. Geophys. Res.* **112**, B09402. doi:10.1029/2007JB004934.
- Davidson J., Turner S., Handley H. and Dosseto A. (2007) Amphibole “sponge” in arc crust? *Geology* **35**, 787–790.
- Defant M. J., Sherman S., Maury R. C., Bellon H., Boer J. D., Davidson J. and Kepezhinskas P. (2001) The geology, petrology, and petrogenesis of Saba Island, Lesser Antilles. *J. Volcanol. Geotherm. Res.* **107**, 87–111.
- DePaolo D. J. (1981) Trace element and isotopic effects of combined wallrock assimilation and fractional crystallization. *Earth Planet. Sci. Lett.* **53**, 189–202.
- Devine J. and Sigurdsson H. (1995) Petrology and eruption styles of Kick'em-Jenny submarine volcano, Lesser Antilles island arc. *J. Volcanol. Geotherm. Res.* **69**, 35–58.
- Devine J. D. (1995) Petrogenesis of the basalt-andesite-dacite association of Grenada, Lesser Antilles island arc, revisited. *J. Volcanol. Geotherm. Res.* **69**, 1–33.
- Dosseto A., Bourdon B., Joron J.-L. and Dupré B. (2003) U–Th–Pa–Ra study of the Kamchatka arc: new constraints on the genesis of arc lavas. *Geochim. Cosmochim. Acta* **67**, 2857–2877.
- Dufek J. and Cooper K. M. (2005) $^{226}\text{Ra}/^{230}\text{Th}$ excess generated in the lower crust: implications for magma transport and storage time scales. *Geology* **37**, 833–836.
- DuFrane S. A., Asmerom Y., Mukasa S. B., Morris J. D. and Dreyer B. M. (2006) Subduction and melting processes inferred from U-series, Sr–Nd–Pb isotope, and trace element data, Bicol and Bataan arcs, Philippines. *Geochim. Cosmochim. Acta* **70**, 3401–3420.
- DuFrane S. A., Turner S., Dosseto A. and Soest M. V. (2009) Reappraisal of fluid and sediment contributions to Lesser Antilles magmas. *Chem. Geol.* **265**, 272–278.
- Elliott T., Plank T., Zindler A., White W. and Bourdon B. (1997) Element transport from slab to volcanic front at the Mariana arc. *J. Geophys. Res.* **102**, 14991–15019.
- Fabbrizio A., Schmidt M. W., Günther D. and Eikenberg J. (2009) Experimental determination of Ra mineral/melt partitioning for feldspars and ^{226}Ra –disequilibrium crystallization ages of plagioclase and alkali-feldspar. *Earth Planet. Sci. Lett.* **280**, 137–148.
- Feineman M. D. and DePaolo D. J. (2003) Steady-state $^{226}\text{Ra}/^{230}\text{Th}$ disequilibrium in mantle minerals: implications for melt transport rates in island arcs. *Earth Planet. Sci. Lett.* **215**, 339–355.
- Garrison J., Davidson J., Reid M. and Turner S. (2006) Source versus differentiation controls on U-series disequilibrium: insights from Cotopaxi Volcano, Ecuador. *Earth Planet. Sci. Lett.* **244**, 548–565.
- George R., Reagan M., Turner S., Gill J. and Bourdon B. (2004) Comment on “Steady-state $^{226}\text{Ra}/^{230}\text{Th}$ disequilibrium in mantle minerals: Implications for melt transport rates in island arcs” by M.D. Feineman and D.J. DePaolo [Earth Planet. Sci. Lett. 215 (2003) 339–355]. *Earth Planet. Sci. Lett.* **228**, 563–567.
- George R., Turner S., Hawkesworth C., Morris J., Nye C., Ryan J. and Zheng S.-H. (2003) Melting processes and fluid and sediment transport rates along the Alaska–Aleutian arc from an integrated U–Th–Ra–Be isotope study. *J. Geophys. Res.* **108**, 2252.
- Gill J. B. (1981) *Orogenic Andesites and Plate Tectonics*. Springer-Verlag.
- Gill J. B., Morris J. D. and Johnson R. W. (1993) Timescale for producing the geochemical signature of island arc magmas: U–Th–Po and Be–B systematics in recent Papua New Guinea lavas. *Geochim. Cosmochim. Acta* **57**, 4269–4283.
- Gill J. B. and Williams R. W. (1990) Th isotope and U-series studies of subduction-related volcanic rocks. *Geochim. Cosmochim. Acta* **54**, 1427–1442.

- Hawkesworth C. J., O'niions R. K. and Arculus R. J. (1979) Nd and Sr isotope geochemistry of island arc volcanics, Grenada, Lesser Antilles. *Earth Planet. Sci. Lett.* **45**, 237–248.
- Heath E., Turner S. P., Macdonald R., Hawkesworth C. J. and Calsteren P. V. (1998) Long magma residence times at an island arc volcano (Soufriere, St. Vincent) in the Lesser Antilles: evidence from ^{238}U – ^{230}Th isochron dating. *Earth Planet. Sci. Lett.* **160**, 49–63.
- Hill E., Wood B. J. and Blundy J. D. (2000) The effect of Ca-Tschermaks component on trace element partitioning between clinopyroxene and silicate melt. *Lithos* **53**, 203–215.
- Huang F., Gao L. and Lundstrom C. C. (2008) The effect of assimilation, fractional crystallization, and ageing on U-series disequilibria in subduction zone lavas. *Geochim. Cosmochim. Acta* **72**, 4136–4145.
- Huang F. and Lundstrom C. C. (2007) ^{231}Pa excesses in arc volcanic rocks: constraint on melting rates at convergent margins. *Geology* **35**, 1007–1010.
- Jarrard R. D. (1986) Relations among subduction parameters. *Rev. Geophys.* **24**, 217–284.
- Keppeler H. (1996) Constraints from partitioning experiments on the composition of subduction zone fluids. *Nature* **380**, 237–240.
- Keppeler H. and Wyllie P. J. (1990) Role of fluids in transport and fractionation of uranium and thorium in magmatic processes. *Nature* **348**, 531–533.
- Knaack C., Cornelius S. and Hooper P. R. (1994) *Trace Element Analysis of Rocks and Minerals. Open File Report*. Department of Geology, Washington State University.
- Knaack C. M. (2003) REE and trace element analysis of rocks and minerals by ICP-MS using a combined fusion-dissolution. In *5th International Conference on the Analysis of Geological and Environmental Materials, Rovaniemi, Finland*.
- Koornneef J. M., Stracke A., Aciego S., Reubi O. and Bourdon B. (2010) A new method for U–Th–Pa–Ra separation and accurate measurement of ^{234}U – ^{230}Th – ^{231}Pa – ^{226}Ra disequilibria in volcanic rocks by MC-ICPMS. *Chem. Geol.* **277**, 30–41.
- Latourrette T., Hervig R. L. and Holloway J. R. (1995) Trace element partitioning between amphibole, phlogopite, and basanite melt. *Earth Planet. Sci. Lett.* **135**, 13–30.
- Lundstrom C. C. (2003) Uranium series disequilibria in mid-ocean ridge basalts: observations and models of basalt genesis. *Rev. Mineral. Geochem.* **52**, 175–214.
- Lundstrom C. C., Shaw H. F., Ryerson F. J., Phinney D. L., Gill J. B. and Williams Q. (1994) Compositional controls on the partitioning of U, Th, Ba, Pb, Sr and Zr between clinopyroxene and haplobasaltic melts: implications for uranium series disequilibria in basalts. *Earth Planet. Sci. Lett.* **128**, 407–423.
- Macdonald R., Hawkesworth C. J. and Heath E. (2000) The Lesser Antilles volcanic chain: a study in arc magmatism. *Earth Sci. Rev.* **49**, 1–76.
- McDonough W. F. and Sun S.-S. (1995) The composition of the Earth. *Chem. Geol.* **120**, 223–253.
- Mckenzie D. (1985) ^{230}Th – ^{238}U disequilibrium and the melting process beneath ridge axes. *Earth Planet. Sci. Lett.* **72**, 149–157.
- Parkinson I. J. and Arculus R. J. (1999) The redox state of subduction zones: insights from arc-peridotites. *Chem. Geol.* **160**, 409–423.
- Peate D. W. and Hawkesworth C. J. (2005) U series disequilibria: insights into mantle melting and the timescale of magma differentiation. *Rev. Geophys.* **43**, 1–43.
- Pickett D. A. and Murrell M. T. (1997) Observation of ^{231}Pa / ^{235}U disequilibrium in volcanic rocks. *Earth Planet. Sci. Lett.* **148**, 259–271.
- Plank T. and Langmuir C. H. (1998) The chemical composition of subducting sediment and its consequences for the crust and mantle. *Chem. Geol.* **145**, 325–394.
- Price R. C., George R., Gamble J. A., Turner S., Smith I. E. M., Cook C., Hobden B. and Dosseto A. (2007) U–Th–Ra fractionation during crustal-level andesite formation at Ruapehu volcano, New Zealand. *Chem. Geol.* **244**, 437–451.
- Prytulak J., Elliott T., Hoffmann D. L. and Coath C. D. (2008) Assessment of USGS BCR-2 as a reference material for silicate rock U–Pa disequilibrium measurements. *Geostan. Geoanal. Res.* **32**, 55–63.
- Reagan M., Tepley, III, F., Gill J. B., Wortel M. and Hartman B. (2005) Rapid time scales of basalt to andesite differentiation at Anatahan volcano, Mariana Islands. *J. Volcanol. Geotherm. Res.* **146**, 171–183.
- Reagan M. K., Tepley, III, F., Gill J. B., Wortel M. and Garrison J. (2006) Timescales of degassing and crystallization implied by ^{210}Po – ^{210}Pb – ^{226}Ra disequilibria for andesitic lavas erupted from Arenal volcano. *J. Volcanol. Geotherm. Res.* **147**, 135–146.
- Regelous M., Colloerson K. D., Wart A. and Wendt J. I. (1997) Trace element transport rates in subduction zones: evidence from Th, Sr and Pb isotope data for Tonga-Kermadec arc lavas. *Earth Planet. Sci. Lett.* **150**, 291–302.
- Regelous M., Turner S. P., Elliot T. R., Rostami K. and Hawkesworth C. J. (2004) Rapid measurement of femtogram quantities of protactinium in silicate rock samples by multicollector inductively coupled plasma–mass spectrometry. *Anal. Chem.* **76**, 3584–3589.
- Sigmarrsson O., Condomines M., Morris J. D. and Harmon R. S. (1990) Uranium and ^{10}Be enrichments by fluids in Andean arc magmas. *Nature* **346**, 163–165.
- Sigmarrsson O., Chmeleff J., Morris J. and Lopez-Escobar L. (2002) Origin of ^{226}Ra – ^{230}Th disequilibria in arc lavas from southern Chile and implications for magma transfer time. *Earth Planet. Sci. Lett.* **196**, 189–196.
- Sigurdsson H. and Shepherd J. B. (1974) Amphibole-bearing basalts from the submarine volcano Kick'em-Jenny in the Lesser Antilles island arc. *Bull. Volcanol.* **38**, 891–910.
- Sims K. W. W., Gill J. B., Dosseto A., Hoffmann D. L., Lundstrom C. C., Williams R. W., Ball L., Tollstrup D., Turner S., Prytulak J., Glessner J. J. G., Standish J. J. and Elliott T. (2008) An inter-laboratory assessment of the thorium isotopic composition of synthetic and rock reference materials. *Geostan. Geoanal. Res.* **32**, 65–91.
- Speed R. C., Smith-Horowitz P. L., Perch-Nielsen K. S., Saunders J. B. and Sanfilippo A. B. (1993) Southern Lesser Antilles arc platform: pre-Late Miocene stratigraphy, structure, and tectonic evolution. *Geol. Soc. Am. Spec.* **277**, 98.
- Spiegelman M. and Elliott T. (1993) Consequences of melt transport for uranium series disequilibrium in young lavas. *Earth Planet. Sci. Lett.* **118**, 1–20.
- Tepley, III, F. J., Lundstrom C. C., Sims K. W. W. and Hekinian R. (2004) U-series disequilibria in MORB from the Garrett Transform and implications for mantle melting. *Earth Planet. Sci. Lett.* **223**, 79–97.
- Thirlwall M. F., Graham A. M., Arculus R. J., Harmon R. S. and Macpherson C. G. (1996) Resolution of the effects of crustal assimilation, sediment subduction, and fluid transport in island arc magmas; Pb–Sr–Nd–O isotope geochemistry of Grenada, Lesser Antilles. *Geochim. Cosmochim. Acta* **60**, 4785–4810.
- Thomas R. B., Hirschmann M. M., Cheng H., Reagan M. K. and Edwards R. L. (2002) (^{231}Pa / ^{235}U)–(^{230}Th / ^{238}U) of young mafic volcanic rocks from Nicaragua and Costa Rica and the influence of flux melting on U-series systematics of arc lavas. *Geochim. Cosmochim. Acta* **66**, 4287–4309.
- Toothill J., Williams C. A., Macdonald R., Turner S. P., Rogers N. W., Hawkesworth C. J., Jerram D. A., Ottley C. J. and Tindle A. G. (2007) A complex petrogenesis for an arc magmatic suite, St. Kitts, Lesser Antilles. *J. Petrol.* **48**, 3–42.

- Touboul M., Bourdon B., Villemant B., Boudon G. and Joron J.-L. (2007) ^{238}U – ^{230}Th – ^{226}Ra disequilibria in andesitic lavas of the last magmatic eruption of Guadeloupe Soufriere, French Antilles: processes and timescales of magma differentiation. *Chem. Geol.* **246**, 181–206.
- Turner S., Bourdon B. and Gill J. (2003) U-series isotopes and magma genesis at convergent margins. *Rev. Mineral. Geochem.* **52**, 255–315.
- Turner S., Bourdon B., Hawkesworth C. and Evans P. (2000) ^{226}Ra – ^{230}Th evidence for multiple dehydration events, rapid melt ascent and the time scales of differentiation beneath the Tonga-Kermadec island arc. *Earth Planet. Sci. Lett.* **179**, 581–593.
- Turner S., Evans P. and Hawkesworth C. (2001) Ultrafast source-to-surface movement of melt at island arcs from ^{226}Ra – ^{230}Th systematics. *Science* **292**, 1363–1366.
- Turner S. and Foden J. (2001) U, Th and Ra disequilibria, Sr, Nd and Pb isotope and trace element variations in Sunda arc lavas: predominance of a subducted sediment component. *Contrib. Mineral. Petrol.* **142**, 43–57.
- Turner S. and Hawkesworth C. (1997) Constraints on flux rates and mantle dynamics beneath island arcs from Tonga-Kermadec lava geochemistry. *Nature* **389**, 568–573.
- Turner S. and Hawkesworth C. (1998) Using geochemistry to map mantle flow beneath the Lau Basin. *Geology* **26**, 1019–1022.
- Turner S., Hawkesworth C., Calsteren P. V., Heath E., Macdonald R. and Black S. (1996) U-series isotopes and destructive plate margin magma genesis in the Lesser Antilles. *Earth Planet. Sci. Lett.* **142**, 191–207.
- Turner S., Hawkesworth C., Rogers N., Bartlett J., Worthington T., Hergt J., Pearce J. and Smith I. (1997) ^{238}U – ^{230}Th disequilibria, magma petrogenesis, and flux rates beneath the depleted Tonga-Kermadec island arc. *Geochim. Cosmochim. Acta* **61**, 4855–4884.
- Turner S., Mcdermott F., Hawkesworth C. and Kepezhinskas P. (1998) A U-series study of lavas from Kamchatka and the Aleutians: constraints on source composition and melting processes. *Contrib. Mineral. Petrol.* **133**, 217–234.
- Turner S., Regelous M., Hawkesworth C. and Rostami K. (2006) Partial melting processes above subducting plates: constraints from ^{231}Pa – ^{235}U disequilibria. *Geochim. Cosmochim. Acta* **70**, 480–503.
- Turner S. P., Peate D. W., Hawkesworth C. J., Eggins S. M. and Crawford A. J. (1999) Two mantle domains and the time scales of fluid transfer beneath the Vanuatu arc. *Geology* **27**, 963–966.
- Turner S., Black S. and Berlo K. (2004) ^{210}Pb – ^{226}Ra and ^{228}Ra – ^{232}Th systematics in young arc lavas: implications for magma degassing and ascent rates. *Earth Planet. Sci. Lett.* **227**, 1–16.
- Van Orman J. A., Saal A. E., Bourdon B. and Hauri E. H. (2006) Diffusive fractionation of U-series radionuclides during mantle melting and shallow-level melt–cumulate interaction. *Geochim. Cosmochim. Acta* **70**, 4797–4812.
- Vigier N., Bourdon B., Joron J. L. and Allegre C. J. (1999) U-decay series and trace element systematics in the 1978 eruption of Ardoukoba, Asal rift: timescale of magma crystallization. *Earth Planet. Sci. Lett.* **174**, 81–97.
- Wadge G. and Shepherd J. B. (1984) Segmentation of the Lesser Antilles subduction zone. *Earth Planet. Sci. Lett.* **71**, 297–304.
- Williams R. W. and Gill J. B. (1989) Effects of partial melting on the uranium decay series. *Geochim. Cosmochim. Acta* **53**, 1607–1619.
- Williams R. W. and Perrin R. E. (1989) Measurement of ^{231}Pa – ^{235}U disequilibrium in young volcanic rocks by mass spectrometry. *EOS Trans. Am. Geophys. Union* **70**(43), 1398.
- Wood B. J., Blundy J. D. and Robinson J. A. C. (1999) The role of clinopyroxene in generating U-series disequilibrium during mantle melting. *Geochim. Cosmochim. Acta* **63**, 1613–1620.
- Yokoyama T., Kobayashi K., Kuritani T. and Nakamura E. (2003) Mantle metasomatism and rapid ascent of slab components beneath island arcs: evidence from ^{238}U – ^{230}Th – ^{226}Ra disequilibria of Miyakejima volcano, Izu arc, Japan. *J. Geophys. Res.* **108**(B7), 2329. doi:10.1029/2002JB002103.
- Zajacz Z. and Halter W. (2007) LA-ICPMS analyses of silicate melt inclusions in co-precipitated minerals: quantification, data analysis and mineral/melt partitioning. *Geochim. Cosmochim. Acta* **71**, 1021–1040.
- Zellmer G., Turner S. and Hawkesworth C. (2000) Timescales of destructive plate margin magmatism new insights from Santorini, Aegean volcanic arc. *Earth Planet. Sci. Lett.* **174**, 265–281.
- Zellmer G. F., Hawkesworth C. J., Sparks R. S. J., Thomas L. E., Harford C. L., Brewer T. S. and Loughlin S. C. (2003) Geochemical evolution of the Soufriere Hills volcano, Montserrat, Lesser Antilles volcanic arc. *J. Petrol.* **44**, 1349–1374.

Associate editor: Frederick A. Frey